SANDIA REPORT
SAND2002-0085
Unlimited Release
Printed January 2002

Preparation Effects on the Performance of Silica-Doped Hydrous Titanium Oxide (HTO:Si)-Supported Pt Catalysts for Lean-Burn NOx Reduction by Hydrocarbons

Timothy J. Gardner, Linda I. McLaughlin, Deborah L. Mowery, and Ronald S. Sandoval

Prepared by
Sandia National Laboratories
Albuquerque, New Mexico 87185 and Livermore, California 94550

Sandia is a multiprogram laboratory operated by Sandia Corporation, a Lockheed Martin Company, for the United States Department of Energy under Contract DE-AC04-94AL85000.

Issued by Sandia National Laboratories, operated for the United States Department of Energy by Sandia Corporation.

Available to DOE and DOE contractors from
U.S. Department of Energy
Office of Scientific and Technical Information
P.O. Box 62
Oak Ridge, TN 37831

Telephone: (865)576-8401
Facsimile: (865)576-5728
E-Mail: reports@adonis.osti.gov
Online ordering: http://www.doe.gov/bridge

Available to the public from
U.S. Department of Commerce
National Technical Information Service
5285 Port Royal Rd
Springfield, VA 22161

Telephone: (800)553-6847
Facsimile: (703)605-6900
E-Mail: orders@ntis.fedworld.gov
Online order: http://www.ntis.gov/ordering.htm

SAND2002-0085
Unlimited Release
Printed January, 2002

Preparation Effects on the Performance of Silica-Doped Hydrous Titanium Oxide (HTO:Si)-Supported Pt Catalysts for Lean-Burn NOx Reduction by Hydrocarbons

Timothy J. Gardner, Linda I. McLaughlin, Deborah L. Mowery, and Ronald S. Sandoval
Materials Chemistry Department

Sandia National Laboratories
P.O. Box 5800, MS 1349
Albuquerque, NM 87185

Abstract

This report describes the development of bulk hydrous titanium oxide (HTO)- and silica-doped hydrous titanium oxide (HTO:Si)-supported Pt catalysts for lean-burn NOx catalyst applications. The effects of various preparation methods, including both anion and cation exchange, and specifically the effect of Na content on the performance of Pt/HTO:Si catalysts, were evaluated. Pt/HTO:Si catalysts with low Na content (< 0.5 wt.%) were found to be very active for NOx reduction in simulated lean-burn exhaust environments utilizing propylene as the major reductant species. The activity and performance of these low Na Pt/HTO:Si catalysts were comparable to supported Pt catalysts prepared using conventional oxide or zeolite supports. In ramp down temperature profile test conditions, Pt/HTO:Si catalysts with Na contents in the range of 3-5 wt.% showed a wide temperature window of appreciable NOx conversion relative to low Na Pt/HTO:Si catalysts. Full reactant species analysis using both ramp up and isothermal test conditions with the high Na Pt/HTO:Si catalysts, as well as diffuse reflectance FTIR studies, showed that this phenomenon was related to transient NOx storage effects associated with $NaNO_2/NaNO_3$ formation. These nitrite/nitrate species were found to decompose and release NOx at temperatures above 300°C in the reaction environment (ramp up profile). A separate NOx uptake experiment at 275°C in $NO/N_2/O_2$ showed that the Na phase was inefficiently utilized for NOx storage. Steady state tests showed that the effect of increased Na content was to delay NOx light-off and to decrease the maximum NOx conversion. Similar results were observed for high K Pt/HTO:Si catalysts, and the effects of high alkali content were found to be independent of the sample preparation technique. Catalyst characterization (BET surface area, H_2 chemisorption, and transmission electron microscopy) was performed to elucidate differences between the HTO- and HTO:Si-supported Pt catalysts and conventional oxide- or zeolite-supported Pt catalysts.

Contents

	Page
Abstract	3
Contents	4
List of Tables	4
List of Figures	5
Introduction	6
Experimental Procedure	7
HMO Support Synthesis	7
Supported Pt Catalyst Preparation	7
Cation Exchange	8
Anion Exchange	9
Control (Benchmark) Catalyst Preparation	9
Post-Preparation Processing and Characterization	9
Catalyst Testing Procedure	10
Results and Discussion	11
Low Na Pt/HTO:Si Catalysts	11
High Na Pt/HTO:Si Catalysts	14
Comparison to Other Supported Pt Catalysts	21
Summary	26
Acknowledgments	27
References	27

List of Tables

		Page
1	Catalyst Description, Composition, and Characterization Data	32

List of Figures

		Page
1	Conversion profiles for all species (CO, C_3H_6, C_3H_8, and NOx) for a low Na (0.04 wt.%) 1.12 wt.% Pt/HTO:Si powder tested in a ramp down mode at a space velocity of 20,000 h^{-1}.	33
2	NOx conversion profiles for a low Na (0.04 wt.%) 1.12 wt.% Pt/HTO:Si powder tested in ramp up, ramp down, and isothermal steady state modes at a space velocity of 20,000 h^{-1}.	34
3	Conversion profiles for all species (CO, C_3H_6, C_3H_8, and NOx) for an anion exchanged low Na (0.01 wt.% Na) 0.95 wt.% Pt/HTO:Si powder tested in a ramp down mode at a space velocity of 20,000 h^{-1}.	35
4	NOx conversion profiles comparing a low Na (0.22 wt.% Na) 1.10 wt.% Pt/HTO:Si powder with two high Na (nominal 3.8 wt.% Na) Pt/HTO:Si powders (nominal Pt loading of 1.0 wt.%) tested in ramp down modes at a space velocity of 20,000 h^{-1}.	36
5	Conversion profiles for all species (CO, C_3H_6, C_3H_8, and NOx) for a high Na (3.89 wt.%) 0.90 wt.% Pt/HTO:Si powder tested in a ramp down mode at a space velocity of 20,000 h^{-1}.	37
6	NOx conversion profiles for sequential ramp up and ramp down experiments using a high Na (3.89 wt.%) 0.90 wt.% Pt/HTO:Si catalyst and a space velocity of 20,000 h^{-1}.	38
7	NOx conversion profiles for isothermal experiments using a space velocity of 20,000 h^{-1} and nominal 1 wt.% Pt/HTO:Si catalysts with various Na contents.	39
8	Diffuse reflectance FTIR spectra for high Na Pt/HTO:Si catalysts (as-calcined vs. after NOx uptake experiment) and various control samples.	40
9	NOx conversion profiles for various supported Pt catalysts with a nominal Pt loading of 1.0 wt.%.	41
10	TEM photomicrographs of low Na (0.29 wt.%) 1.09 wt.% Pt/HTO:Si catalyst, including inset electron diffraction pattern representative of TiO_2 support phase.	42
11	TEM photomicrograph of high Na (3.70 wt.%) 0.94 wt.% Pt/HTO:Si catalyst, including inset electron diffraction pattern representative of large single crystal ([112] orientation]) Pt particles.	43
12	EDS spectrum of support phase composition for high Na (3.70 wt.%) 0.94 wt.% Pt/HTO:Si catalyst.	44
13	TEM photomicrographs of low Na (0.01 wt.%) 0.95 wt.% Pt/HTO:Si catalyst produced by anion exchange.	45
14	TEM photomicrograph of low Na (0.10 wt.%) 1.11 wt.% Pt/HTO catalyst, including inset electron diffraction pattern representative of TiO_2 support phase.	46

Introduction

The EPA has recently announced new Tier 2 emissions standards for personal vehicles that are scheduled to begin phase-in by 2004. These proposed new standards call for sharp reductions in nitrogen oxide (NOx), carbon monoxide (CO), hydrocarbon (HC), and particulate matter (PM) emissions, in addition to increasing the catalyst durability requirement to 120,000 miles. It is important to point out that these Tier 2 emissions standards will apply to all on-highway personal vehicles, including both gasoline- and diesel-engine powered automobiles (passenger cars), light-duty trucks, and sport utility vehicles with a gross vehicle weight < 10,000 lbs [1]. This means that vehicles currently exempt from Tier 1 emission standards, including nearly all diesel-engine powered vehicles, will require the development of new catalyst materials to meet the sharp reduction in pollutants required by the Tier 2 standards. The combination of future emissions requirements and additional government-mandated increases in fuel efficiency leads to the current motivation to develop emissions control solutions for lean-burn gasoline- or diesel engine-powered vehicles. "Lean-burn" engines run at much higher air-to-fuel ratios than conventional gasoline engines and offer fuel economy advantages due to more efficient combustion. However, catalytic NOx reduction in the oxidizing exhaust environment produced by these engines is much more difficult, and requires the development of novel remediation technologies, including new catalyst systems.

Several emissions control strategies exist for NOx reduction in net oxidizing environments, also commonly referred to as lean-NOx catalysis. Primary lean-NOx catalysis options include passive lean-NOx catalysis, active lean-NOx catalysis, and selective catalytic reduction (SCR) [2]. Passive lean-NOx systems utilize only unburned hydrocarbons present in the exhaust stream to affect NOx reduction. Active lean-NOx systems involve reductant (e.g., fuel or other tailored hydrocarbon) addition to the exhaust stream to affect NOx reduction. Finally, selective catalytic reduction (SCR) involves the addition of a specific reductant (e.g., urea or ammonia), which is very selective for NOx reduction in oxidizing environments. This paper deals with catalyst development for the active lean-NOx approach to NOx reduction in oxidizing environments. Other technology options for NOx removal include NOx adsorber catalysts, which combine NOx storage and catalysis functionalities [3,4], and plasma-based processes [5].

Because Pt-based catalysts are active at relatively low temperatures for active lean-NOx catalysis, numerous studies have identified these materials as excellent candidates for light- (and medium-) duty diesel exhaust applications [6-12]. This study will examine novel hydrous metal oxide-supported Pt catalysts for active lean-NOx catalysis. Hydrous metal oxides (HMOs) are chemically synthesized materials that contain a homogeneous distribution of ion exchangeable alkali cations, which provide charge compensation to the metal-oxygen framework. Both the presence of these alkali cations and the resulting high cation exchange capacities clearly set these materials apart from conventional precipitated hydrous oxides [13,14]. These novel materials have many desirable characteristics for catalyst support applications, including high cation exchange capacity, anion exchange

capability, high surface area, ease of adjustment of acidity and basicity, bulk or thin film preparation, and similar chemistry for preparation of various transition metal oxides (e.g., TiO_2, ZrO_2, Nb_2O_5, and Ta_2O_5) [15-17]. Their high ion exchange capacity and high surface area facilitate the preparation of highly dispersed heterogeneous catalysts with high active phase loadings [18-19], which, combined with their flexibility of preparation (bulk or thin film preparation) [20], makes them ideally suited for the fabrication of automotive exhaust catalysts [21-23]. These advantages have previously been exploited to develop a variety of heterogeneous catalysts for coal liquefaction and hydrotreating applications [24-28].

In an earlier screening study related to active lean-burn NOx catalysis, silica-doped hydrous titanium oxide (HTO:Si)-supported Pt catalyst materials were identified as promising catalysts worthy of further examination [11]. Here we compare nominal 1 wt.% Pt/HTO and Pt/HTO:Si catalysts prepared via cation or anion exchange relative to supported Pt catalysts on a range of commercial oxide or zeolite supports. A major thrust of this work involved the evaluation of the effect of the Na^+ content of Pt/HTO:Si catalysts on their performance for lean-burn NOx reduction. This work is intended to complement recent work at General Motors Research and Development Center with similar catalyst materials [29].

Experimental Procedure

HMO Support Synthesis

A minimum of three steps are required to prepare HMO-supported catalysts. The first two steps involve the preparation of an ion exchangeable catalyst support material via sol-gel techniques. The key feature of this preparation is the incorporation of cation exchangeable Na^+ cations into the structure of the HMO material. Detailed HMO ion exchangeable catalyst support synthesis procedures have been previously reported [11,15-17,25] and will not be discussed herein. The third step of HMO-supported catalyst preparation involves an ion exchange procedure wherein catalyst precursor ions are incorporated via ion exchange or adsorption mechanisms [18,25]. These ion exchange procedures and the associated process variables will be discussed extensively herein. Finally, an activation procedure is required to convert the catalyst precursor to the final active phase.

The Na^+ form HTO:Si support was synthesized with a Na:Ti ratio of 0.5 and Ti:Si ratio of 0.2, yielding a bulk ion exchanger with an empirical formula of $NaTi_2Si_{0.4}O_{5.8}H$. A Na^+ form HTO support with a Na:Ti ratio of 0.5 was also synthesized, yielding a bulk ion exchanger with an empirical formula of $NaTi_2O_5H$. Significant acidification and ion exchange studies have been previously reported with similar materials [18,25].

Supported Pt Catalyst Preparation

For all catalyst preparation, Pt loadings were nominally targeted at 1 wt.% on a calcined basis. Standard procedures were utilized for both cation exchange [11,22,23] and anion exchange/adsorption [22,23] of charged Pt precursor species.

Cation Exchange

Cation exchange was performed by adding the bulk Na^+ form HTO or HTO:Si support to an aqueous platinum tetraammine nitrate ($Pt(NH_3)_4(NO_3)_2$) solution. The resulting slurry (pH > 10) was then stirred while acidifying with nitric acid (HNO_3) to pH 5.5 in order to affect cation exchange while also removing a substantial fraction of Na^+ from the bulk ion exchanger. Following a 10 minute (min) mixing period at pH 5.5, the solids were separated from the liquid phase by filtering with a coarse porosity glass frit Buchner funnel. The solids were washed with deionized water, then acetone, and finally dried under house vacuum (7.5-12.5 mm Hg) at room temperature. Because of the high cation exchange capacity of these materials (3-5 milliequivalents/g, corresponding to 6-10 wt.% Na^+ in as-prepared form), and the relatively low metal loading targets used to prepare these catalysts, it is not surprising that significant amounts of residual Na^+ (3-5 wt.%) remained in the HTO:Si material after this cation exchange step. This preparation was used to synthesize the standard high Na Pt/HTO:Si catalyst.

In order to prepare low Na Pt/HTO and Pt/HTO:Si catalysts (defined as $\leq$ 0.5 wt.% Na on a calcined basis), an acidification procedure was used following the cation exchange procedure to remove residual, unexchanged Na^+ ions from the cation-exchanged HTO or HTO:Si material. The acidification procedure involved redispersing the solids collected by filtration after cation exchange in deionized H_2O. Acidification was performed by adding HNO_3 to the resulting slurry until a pH of 4 was obtained. This pH value is very close to the isoelectric point of the HTO/HTO:Si material, where complete H^+ for Na^+ exchange should be accomplished. The slurry was held at pH 4 for ~1 min, with additional HNO_3 added as necessary. A filtering procedure similar to that described above was used to separate the solids from the liquid phase. This overall acidification procedure was then repeated as necessary until the pH of the redispersed cation-exchanged HTO or HTO:Si was ~4, indicating that Na^+ removal was essentially complete. Following the final filtration step, the filtered solid was washed with water and then acetone, followed by room temperature drying under house vacuum as described previously.

In addition to the standard high Na Pt/HTO:Si preparation technique described above, an alternate high Na Pt/HTO:Si catalyst was prepared via incipient wetness impregnation of a low Na Pt/HTO:Si catalyst (in its final calcined form) with sodium nitrate ($NaNO_3$). Following drying and calcination, this preparation yielded a composition similar to a standard high Na Pt/HTO:Si catalyst. The major difference between the preparation of the two high Na materials was the potential nature of the interaction between the Na phase and the active Pt phase. Since a single calcination procedure was used in the case of the standard preparation, Pt particles form in conjunction with the dispersion of the Na

phase. For the alternate high Na Pt/HTO:Si preparation, the Na precursor was added to a previously calcined low Na Pt/HTO:Si sample. In this case, the Pt particles already existed in a dispersed state on the HTO:Si support prior to impregnation with the Na precursor. A second calcination was used to convert the Na precursor and disperse the Na phase. Comparing these two preparation techniques was important to determine if the effect of the high Na content was general or somehow related to catalyst preparation.

Anion Exchange

Anion exchange techniques varied significantly from cation exchange techniques, both in terms of metal precursor and solution conditions. First, an aqueous slurry of the Na^+ form HTO:Si support in water was acidified to pH 2.5 via the addition of hydrochloric acid (HCl). In addition to ion exchanging virtually all of the Na^+ (with H^+) in the original ion exchangeable support, lowering the pH to less than the isoelectric point (pH 4-5) of the HTO:Si material develops a positive surface charge on the particles, which facilitates anion adsorption for charge compensation purposes. The slurry was then filtered and washed with deionized water as described previously. Similar to the acidification procedure described above, the filter cake was redispersed into an aqueous slurry and reacidified until a stable redispersion pH of less than 2.7 was achieved, indicating complete acidification of the HTO:Si support. Upon achieving the desired acidity, a proper quantity of chloroplatinic acid (H_2PtCl_6), corresponding to 20% excess by weight over the desired final Pt loading, was added to the nominal pH 2.5 slurry. Following a 30 min mixing period the slurry was then filtered, rinsed with deionized water, and rinsed with acetone, with the remaining solids dried at room temperature under house vacuum as described previously.

Control (Benchmark) Catalyst Preparation

Nominal 1 wt.% Pt catalysts supported on conventional oxides were prepared via incipient wetness impregnation using an aqueous solution of $Pt(NH_3)_4(NO_3)_2$, followed by drying at both room temperature and 100°C. TiO_2 (Degussa P25, 45 m^2/g surface area) and SiO_2 (Cabosil HS-5, 300 m^2/g surface area) were used as the oxide supports for these benchmark catalysts. Also included as benchmark materials were a Pt/Al_2O_3 catalyst synthesized using a Pt dinitrodiammine ($Pt(NH_3)_2(NO_3)_2$) precursor [30] and a Pt/ZSM-5 material, both of which were obtained from a catalyst supplier.

Post-Preparation Processing and Characterization

Samples of the as-prepared catalyst precursor powders were analyzed for Na and Pt via Atomic Absorption Spectrophotometry (AAS) following dissolution of these materials in concentrated HCl. All catalyst powders were pressed into disks at 12 kpsi, lightly ground with a mortar and pestle, and sieved to a size range of -60/+80 mesh. The granules were then calcined at 600°C for 2 hours (h) at a heating rate of 5°C/min in stagnant air. A volatiles analysis was performed on the as-prepared catalyst precursor powder by determining the weight loss after a similar calcination procedure. Volatile contents typically ranged from 20-30 wt.% in the as-prepared materials, largely consisting of water and acetone. The AAS results were combined with the volatiles analysis results in order to calculate accurate Pt and Na loadings for all of the respective catalysts on a calcined

basis. Unless otherwise specified, catalyst compositions will be reported in this manner throughout this report.

Several techniques were used to characterize the supported Pt catalyst samples. X-ray diffraction was performed at room temperature on a Siemens D-500 diffractometer with a θ-θ sample geometry and Cu K_α radiation between 2θ = 10 to 60°. Data reduction was performed using Siemens D-500 software. These x-ray analyses were performed with the knowledge that specific data regarding the crystalline state of the active catalyst phase might be impossible to obtain due to the small quantities (< 5 wt.%) of these phases. Transmission electron microscopy (TEM) was performed using a Philips CM30 instrument operating at 300 kV, with a point-to-point resolution of 0.23 nm. Sample preparation involved dispersing powder samples on Cu grids containing holey carbon films by dipping the grid directly into a mixture of the catalyst powder and butanol which had been ground using a mortar and pestle. More extensive evaluation of certain samples was performed using a Hitachi HF2000 TEM equipped with a field emission gun at Oak Ridge National Laboratory. These samples were prepared by first embedding granulated powders in potting material, followed by fabrication of powder cross-section samples by slicing, grinding, dimpling, and ion milling procedures. This type of sample preparation allowed for viewing of extensive thin areas of a respective sample rather than the thick regions typically obtained in a crushed powder specimen. Surface area measurements were performed on a Quantachrome Autosorb 6B unit using the BET method. H_2 chemisorption measurements were performed on the supported Pt catalysts using a Coulter Omnisorp Apparatus. Prior to measurement of the H_2 uptake, the catalysts were reduced in situ at 400°C for 2h in flowing H_2. Determination of the H_2 chemisorption capacity was made by linear extrapolation of the data taken in the 50 to 300 mm Hg region to zero pressure. Although total, reversible, and irreversible adsorption isotherms were determined for each material, only the total H_2 chemisorption capacity was used to compare these different materials. Also, a Nicolet 20SXB Fourier transform infrared spectrometer (FTIR) equipped with a SpectraTech COLLECTOR™ diffuse reflectance accessory was used to obtain FTIR spectra of various catalyst and control samples involved in this study. For FTIR characterization, a 20 wt.% sample and 80 wt.% potassium bromide (KBr) mixture was used in all cases.

Catalyst Testing Procedure

The catalysts were evaluated using a simulated lean-burn gasoline exhaust formulation for reduction of NOx and oxidation of propane (C_3H_8), propylene (C_3H_6), and CO. In the catalyst evaluation unit, the following gases (or gas mixtures) were blended on-line via mass flow controllers: N_2, air, carbon dioxide (CO_2), $CO/H_2/N_2$, nitric oxide (NO)/N_2, and $C_3H_8/C_3H_6/N_2$. Steam was added by passing the air stream through a heated bubbler containing H_2O. The six gas streams were mixed via a static mixer and passed through a horizontal furnace containing a quartz tube (13 mm ID) with a packed bed catalyst (~1.5 g) held in place with quartz wool plugs. The feed gas composition used for all of the experiments in this work was the following: 7% CO_2, 8% O_2, 7% H_2O, 400 ppm CO, 133 ppm H_2, 250 ppm NO, 525 ppm C_3H_6, 175 ppm C_3H_8, and balance N_2. The bulk materials were evaluated at 20,000 standard cubic centimeters (scc) feed gas per h per cc

of catalyst material, equivalently expressed as 20,000 h^{-1}. Temperature was measured via a thermocouple positioned at the approximate midpoint of the catalyst bed just outside of the quartz reactor tube. The gas streams (feed and product) were analyzed with an on-line gas chromatograph (Agilent Technologies) for CO (Molecular Sieve 5A column), C_3H_8 (Poraplot Q column), and C_3H_6 (Poraplot Q column), and with a chemiluminescence analyzer (Antek Industrial Instruments) for NOx (as total NO + nitrogen dioxide [NO_2]). Unfortunately, it was not possible with our analytical capabilities to determine the individual yields of NOx to either nitrous oxide (N_2O) or N_2.

Several different types of temperature profiles were used to evaluate the catalytic activity of the materials. "Ramp down" test mode experiments were conducted by increasing the temperature to 500°C under N_2, passing the feed gas over the catalyst, and then lowering the temperature to at least 200°C at a rate of 5°C/min or less. For comparison purposes, the catalyst was evaluated under similar conditions as a function of increasing temperature. For this "ramp up" test mode, the furnace was first held at 150°C for 20 min and then ramped to 500°C at 5°C/min. Typically, NOx readings were taken every 30 seconds, while gas chromatograph injections were performed every 5 min. Steady state isothermal measurements of catalyst activity were also made in an increasing temperature mode. Isothermal catalyst activity measurements were taken by holding the temperature constant for a minimum of 15 min (actual range 15-60 min), with NOx, CO, C_3H_8, and C_3H_6 concentrations averaged over the last 10 min of the isothermal hold to determine conversions. In certain cases, extended isothermal experiments (2-3 h) were performed to either confirm steady state data or to evaluate the NOx adsorption capacity of respective samples.

Results and Discussion

Representative catalyst compositions, as well as catalyst characterization data, are given in Table 1 for the range of materials evaluated in this study.

Low Na Pt/HTO:Si Catalysts

It was assumed that unexchanged Na^+ remaining on the HTO:Si support might be detrimental to catalyst performance. Therefore, it was standard procedure to utilize acidification techniques to remove this residual Na^+ prior to final catalyst activation and testing. One of the highest activity catalysts identified in our initial screening studies [11] was a low Na Pt/HTO:Si formulation with a nominal Pt loading of 1.0 wt.%. The conversion profiles obtained for the various simulated lean-burn gasoline exhaust gas species using a ramp down test with a typical low Na Pt/HTO:Si catalyst formulation are shown in Figure 1.

Three possible reductants are present in the simulated lean-burn gasoline exhaust gas mix that could facilitate reduction of NOx in the net oxidizing environment, CO, C_3H_6, and C_3H_8. These three species provide effective HC:NOx ratios (expressed on a unit carbon basis) of 1.6:1 (CO), 6.3:1 (C_3H_6), and 2.1:1 (C_3H_8). Simply from a concentration basis, one would expect C_3H_6 to be the most significant species involved in NOx reduction for

this simulated lean-burn gasoline exhaust gas mix. This is consistent with a wealth of information in the published literature regarding the effectiveness of NOx reduction via small alkenes in oxidizing environments [6,9,31-35].

A definitive understanding of the kinetics and mechanisms of NOx reduction over supported Pt catalysts by hydrocarbons in realistic lean-burn automotive exhaust environments does not currently exist. The complex chemical environments typical of an automotive exhaust stream have generally only been evaluated in more applied screening or durability studies [6,11,12,32,36-40]. Virtually all mechanistic studies to date related to active lean-NOx catalysis have involved simple, high purity feed-gas mixtures (often including only a single hydrocarbon reductant). These studies have resulted in several postulated mechanisms for lean-burn NOx reduction that involve: 1) oxidation of NO to NO_2, which then reacts with hydrocarbons [41-43]; 2) formation of a highly reactive, partially oxidized hydrocarbon intermediate [7,36,44,45]; 3) formation of an intermediate species containing both carbon and nitrogen [41,46-49]; and 4) reduction of the metal surface followed by NO dissociation on the metal [9,10,30,42,43,50]. Substantial evidence has shown the existence of unique, hydrocarbon-dependent NOx reduction mechanisms involving various contributions of the catalyst support and/or the Pt particles [42,43,50]. Overall, the determination of specific reaction mechanisms has been hindered by the lack of identification of reaction intermediate species.

Even a cursory examination of Figure 1 highlights the coincidence of the C_3H_6 and NOx conversion profiles. For the purposes of quantitatively comparing conversion profiles within this report, the light-off temperature (T_{50}) is defined as the temperature where the conversion of a given species reaches 50% of its maximum value. As the C_3H_6 conversion achieves light-off (T_{50} = 171°C), the NOx conversion profile reaches its maximum value. This result is consistent with many literature reports related to NOx reduction via C_3H_6 (or ethylene [C_2H_4]) in oxidizing environments [6,7,9,30,34,35]. Beyond this temperature, C_3H_6 conversion remains at 100%, while NOx conversion begins to decrease with increasing reaction temperature. Processing effect studies on supported Pt catalysts have shown that certain process variables (e.g., support, Pt precursor, and Pt loading/dispersion) can shift the maximum NOx conversion and NOx conversion profile to higher or lower temperature [9,10,30,35,51]. Of significance is the fact that the C_3H_6 conversion profile undergoes a corresponding shift along with the NOx conversion profile. This lends further credence to the supposition that C_3H_6 is the dominant reductant species involved in the NOx reduction reaction mechanism for this simulated exhaust gas formulation.

The overall shape of the NOx conversion profile is interesting since it is significantly different than the conversion profiles for CO, C_3H_6, and C_3H_8. The NOx conversion profile reaches a maximum in conversion with increasing temperature, followed by a decrease in conversion as temperature is further increased. At higher temperatures (greater than the temperature of maximum NOx conversion), NOx conversion begins to decrease even though C_3H_6 conversion remains at 100%. This is a common feature of all active lean-NOx catalytic processes. There are several possible explanations for this

behavior, which are consistent with the possible reaction mechanisms described earlier. First, due to the rapidly increasing rate of hydrocarbon combustion in the light-off temperature regime, the partially oxidized hydrocarbon intermediate species required to facilitate NOx reduction might not have sufficient residence time or be available at all to affect NOx reduction at higher temperatures [7]. Second, the distribution of chemisorbed species at the Pt catalyst surface can change significantly as a function of temperature [52]. It should be reiterated that the concentration of O_2 in the exhaust gas mixture is several orders of magnitude higher than that of the NO and hydrocarbon species present. In order to effectively catalyze the NOx reduction process, the adsorption of NO and hydrocarbons at the platinum surface must effectively compete with the adsorption of O_2. It is known that as temperature is increased, the platinum surface has a higher affinity for O_2 than NO. Thus, O_2 can serve effectively as a poison at higher temperatures with platinum catalysts [30,35,50,53].

Although NOx reduction via CO has been extensively studied in the literature with respect to three-way catalysts [54], CO conversion to CO_2 is facile over noble metal catalysts in oxidizing environments. Thus, although CO can play important roles in the NOx reduction mechanism in net neutral or net reducing exhaust environments, it is unlikely that CO significantly participates in the overall NOx reduction mechanism in oxidizing exhaust environments, as long as other hydrocarbons are present in reasonable quantities [6,31,35,36]. This is illustrated in Figure 1 by the fact that the conversion of CO is nearly 100% complete by 150°C, well before any significant NOx conversion is observed.

It is also obvious from Figure 1 that C_3H_8 has little contribution to the overall NOx reduction activity of the low Na Pt/HTO:Si catalyst. Consistent with previous work, appreciable C_3H_8 conversion is not observed until temperatures of 225-250°C (T_{50} = 307°C), with complete conversion not observed until ~400°C [35]. It is therefore possible that some of the high temperature tail associated with the NOx conversion profile might be attributed to NOx reduction via C_3H_8. Several literature reports have discussed NOx reduction over supported Pt catalysts in oxidizing environments utilizing only C_3H_8 as a reductant, with several reaction mechanisms being possible (as described above), involving contributions from the catalyst support and/or the Pt particles. It has been suggested that the chemistry of the support is important, which has been demonstrated by the lack of (or significantly lower) NOx reduction activity using a C_3H_8 reductant observed with either unsupported Pt [55] or a Pt/SiO_2 catalyst (no significant acid sites) [50,56] relative to active Pt/Al_2O_3 catalysts (significant Lewis acid sites) [42,56]. Considerable previous work has shown that the combination of the mixed oxides (TiO_2 and SiO_2) in the HTO:Si support results in significant acidity (both Lewis and Brønsted acid sites) [27,57-61] that might facilitate some activity for NOx reduction via C_3H_8 over Pt/HTO:Si catalysts.

A comparison of the results obtained from the different test modes (ramp up, ramp down, and isothermal) for a repeat low Na Pt/HTO:Si catalyst preparation is shown in Figure 2. For clarity, only the NOx conversion profiles are shown for the various test modes. Note

that the NOx conversion profiles are very similar for the ramp down and isothermal test modes, with only a very slight shift of the NOx conversion profile to higher temperature in the case of the isothermal test. These similar NOx conversion profiles are likely due to the low cooling rate (i.e., furnace cooling) observed at lower temperatures during the ramp-down profile. Under these conditions, the thermal lag between the catalyst sample and the control thermocouple outside the quartz tube would be minimized, and NOx conversion values would be expected to approach steady state (isothermal) values. Possible hydrocarbon adsorption effects in a ramp down test mode should be minimized since the NOx conversion temperature window is approached from high temperature where hydrocarbon conversion is very high. The ramp up test mode resulted in an increased maximum NOx conversion and a shift in the NOx conversion profile to significantly higher temperature (~20-30°C). This behavior is largely consistent with the expected thermal lag between the locally cooler catalyst sample and the locally warmer control thermocouple being most significant at lower temperatures under temperature ramping conditions. This thermal lag would result in an apparent delay in catalyst light-off. Also, during ramp up from low temperature in the simulated exhaust gas mix it is speculated that some hydrocarbon adsorption occurs, which would ultimately result in a higher maximum NOx conversion due to locally increased HC:NOx ratios when hydrocarbon desorption and reaction occur in conjunction with catalyst light-off [62-64]. This hydrocarbon adsorption effect is relatively short-lived; all of the NOx conversion profiles converge by a temperature of 275°C. As expected from the results shown in Figure 1, as well as previous literature reports, the conversion profiles for the other species of interest in the gas mix were similarly affected by the various test modes.

The results for the low Na Pt/HTO:Si catalyst prepared via anion exchange tested using the ramp down profile are shown in Figure 3. This Pt/HTO:Si catalyst had an extremely low residual Na^+ level (0.01 wt.%). The maximum NOx conversion as well as the conversion profiles for all species are very similar to those shown in Figure 1 for the low Na Pt/HTO:Si catalyst prepared by cation exchange followed by acidification. The C_3H_8 light-off is slightly enhanced in the case of the anion exchanged Pt/HTO:Si catalyst (T_{50} = 281°C vs. T_{50} = 315°C), possibly due to the very low Na content of this material or due to increased acidity of this material resulting from acidic chloride (Cl^-) anion adsorption during the acidification/anion exchange preparation.

High Na Pt/HTO:Si Catalysts

High Na Pt/HTO:Si catalysts (3-5 wt.% Na) prepared by two different techniques (standard and incipient wetness impregnation of additional Na to low Na Pt/HTO:Si catalysts) were evaluated in this phase of the study. In certain cases, intermediate Na levels or alternate alkali metals (i.e., K) were also evaluated. Figure 4 shows the comparison of NOx conversion profiles obtained using a ramp down test mode for low Na and high Na Pt/HTO:Si catalysts (both preparation techniques).

The ramp down NOx conversion profile for the low Na Pt/HTO:Si catalyst shown in Figure 4 is very similar to that shown in Figure 2. This comparison shows excellent reproducibility in the test data for replicate catalyst preparation experiments. Figure 4

also includes high Na Pt/HTO:Si catalysts prepared in two different ways, although catalyst performance was similar. First, the high Na Pt/HTO:Si catalysts show an apparent broad NOx conversion window over a relatively wide temperature range (175-375°C for 25% NOx conversion). This is compared to the relatively narrow NOx conversion window obtained with the low Na Pt/HTO:Si catalyst (150-250°C for 25% NOx conversion). Second, the NOx conversion profile for the high Na Pt/HTO:Si catalysts is shifted to slightly higher temperature (T_{50} increases by 15-25°C) relative to the low Na Pt/HTO:Si catalyst. It should be noted that the maximum NOx conversion for the high Na Pt/HTO:Si catalysts is lower than the low Na Pt/HTO:Si catalyst (~50 vs. ~70%). This decrease in the maximum NOx conversion was not viewed as a major issue since the broad NOx conversion temperature window of the high Na Pt/HTO:Si catalyst was a potential advantage relative to the narrow temperature range of appreciable NOx reduction activity typically observed for supported Pt catalysts. These results clearly show that the effect of the high Na content on Pt/HTO:Si catalysts is general with respect to the two different catalyst preparation techniques.

In order to help explain this interesting data, it is instructive to examine the conversion profiles of all of the species of interest for the high Na Pt/HTO:Si catalyst tested in the ramp down mode. This data is shown in Figure 5 for a different high Na Pt/HTO:Si catalyst prepared by the standard technique. This particular catalyst was also evaluated in a separate study at the General Motors Research and Development Center [29]. By comparing Figures 4 and 5, excellent reproducibility is shown with respect to repeatable catalyst performance using the standard high Na Pt/HTO:Si catalyst preparation technique. Relative to the conversion profiles shown in Figure 1 for the low Na Pt/HTO:Si catalyst, significant differences are observed in the case of the individual conversion profiles for the various gas species. As noted above in the discussion of Figure 4, higher temperatures are required to achieve light-off of the NOx conversion profile for the high Na Pt/HTO:Si catalyst (~205°C vs. ~170°C). By comparison of Figures 1 and 5, it is obvious that the light-off of CO, C_3H_6, and C_3H_8 are also affected by the high Na concentration of this catalyst. For the high Na Pt/HTO:Si catalyst, the light-off of C_3H_6 appears to be inhibited the least (T_{50} delayed ~15°C with respect to the low Na sample), while Na has a more significant inhibition role in the light-off behavior of CO (delayed $\geq$ 25°C with respect to the low Na sample) and especially C_3H_8 (delayed ~200°C with respect to the low Na sample). The large delay in the C_3H_8 light-off is consistent with the fact that residual Na in/on the HTO:Si support would be expected to poison the acid sites present [65-67]. The net effects of the shift of the above conversion profiles for the high Na Pt/HTO:Si catalyst are that the CO and C_3H_6 light-off profiles are more similar in temperature, while the NOx and C_3H_6 light-off profiles are farther apart in temperature (with respect to the low Na Pt/HTO:Si catalyst). This suggests a more complex interaction between these species in the case of the high Na Pt/HTO:Si catalysts.

Worthy of note in the discussion of Figure 5 is that NOx conversion is observed for this catalyst at temperatures where both the CO and C_3H_6 species are completely oxidized (> 225°C). This is surprising given the typical results observed for low Na Pt/HTO:Si catalysts (see Figure 1), where NOx conversion begins to decrease at temperatures where

C_3H_6 conversion is complete. The observed low C_3H_8 oxidation activity for the high Na Pt/HTO:Si catalyst also does not correlate with the high apparent NOx conversion observed in the 175-375°C temperature range. Regardless of the possible explanations for this behavior, the broad temperature range of apparent NOx conversion observed for the high Na Pt/HTO:Si catalysts was of significant interest for additional characterization and development activities. As an initial step, high Na Pt/HTO:Si catalysts were also examined using various testing protocols similar to those previously discussed for the low Na Pt/HTO:Si catalysts (see Figure 2).

Unlike the results obtained for the low Na Pt/HTO:Si catalysts, significant differences in performance were observed for high Na Pt/HTO:Si catalysts tested using these various test modes. The results obtained for ramp up vs. ramp down test modes for a high Na Pt/HTO:Si catalyst are shown in Figure 6. The broad temperature range of appreciable NOx conversion shown previously in Figures 4 and 5 for ramp down experiments is also observed in this case (square symbols). However, the NOx conversion profile observed in the case of the ramp up test mode is significantly different (diamond symbols). Similar to the results obtained with the low Na Pt/HTO:Si catalyst using the ramp up test mode (see Figure 2), the initial NOx light-off profile is delayed slightly in the case of the ramp up test mode, with maximum NOx conversion also being higher than in the case of the ramp down test mode. However, in marked contrast to the results observed for the ramp down test mode, the temperature window of appreciable NOx conversion is rather narrow for the high Na Pt/HTO:Si catalyst tested in the ramp up test mode. Instead of the NOx conversion profile returning to a baseline of ~0% conversion at higher temperature, a large negative conversion of NOx is observed at elevated temperature for the ramp up test mode. This is consistent with a significant desorption of NOx from this catalyst material. Apparent NOx conversion did not return to a 0% baseline until very high temperatures (> 450°C). The large area under the negative conversion portion of the curve indicates that this high Na Pt/HTO:Si material has a significant NOx adsorption capacity. Very similar ramp up NOx conversion profiles have been shown for high temperature NOx trap materials [37].

Figures 5 and 6 provide strong evidence for NOx storage phenomena with the high Na Pt/HTO:Si catalyst materials. The ramp down profile data for all species (Figure 5) shows a significant temperature region (225-425°C) where apparent NOx conversion occurs without the presence of hydrocarbon intermediates (CO and C_3H_6 are rapidly oxidized at these temperatures, while C_3H_8 is not oxidized at all), while the ramp up profile NOx data (Figure 7) shows a clear desorption of NOx in the higher temperature portion (300-500°C) of the profile. Since the observed NOx storage effects were possibly related to the transient nature of the dynamic (ramp up or ramp down) test profiles, it was important to examine steady state (isothermal) test profiles to differentiate actual catalytic NOx conversion from NOx adsorption.

Figure 7 shows the NOx conversion profiles obtained using an isothermal test mode for the same low and high Na Pt/HTO:Si catalysts as those shown in Figure 4. Consistent with Figure 4, the results for the two high Na Pt/HTO:Si catalysts prepared via different

techniques are very similar. With respect to the low Na Pt/HTO:Si catalyst results, the NOx conversion profiles for the high Na Pt/HTO:Si catalysts show lower maximum NOx conversion, as well as a shift of the overall NOx conversion profile toward slightly higher temperature. Both of these observations are also consistent with results previously shown for ramp down test profiles (see Figure 4). Observations related to the conversion profiles of the other species (CO, C_3H_6, and C_3H_8) were found to be very similar to those shown previously in Figures 1 and 5 for the low and high Na Pt/HTO:Si catalysts, respectively.

These results clearly show the temperature regime over which actual NOx conversion occurs for the Pt/HTO:Si catalysts with various Na contents. With respect to the high Na Pt/HTO:Si catalyst, significant NOx conversion (defined as $\geq$ 25 %) would only be expected in the 185-225°C temperature range, while the low Na Pt/HTO:Si catalyst shows a temperature range of 165-240°C. These results are in direct contrast to the ramp down test results that showed a much broader temperature range of apparent NOx conversion for the high Na Pt/HTO:Si material. These isothermal test results, together with the ramp up and ramp down results described previously, clearly indicate that the broad range of apparent NOx conversion observed for the high Na Pt/HTO:Si catalyst in the ramp down test was an artifact of transient effects associated with NOx adsorption. Re-examination of the NOx conversion profiles shown in Figure 4 for the high Na Pt/HTO:Si catalysts in light of the isothermal test results might lead one to conclude that the apparent broad window of NOx conversion observed during ramp down profile experiments is the result of the superposition of steady state NOx conversion and NOx storage components.

The combination of NOx adsorber phases with Pt-based catalysts has sparked a recent surge of interest in NOx storage or adsorber catalysts [3,4]. The most efficient NOx adsorber phase reported in the literature is barium oxide (BaO), although other alkali metal oxide or alkaline earth oxide additives can also act as NOx adsorber phases [4,68]. Several studies of supported Pt/BaO adsorber catalysts cycling between lean and rich exhaust conditions have established the following general mechanism to describe NOx adsorber catalyst operation [68-72]. Initially, NO is oxidized to NO_2 on the Pt surface, followed by spillover to the barium phase to form barium nitrate ($Ba(NO_3)_2$). Adsorber regeneration is performed under rich conditions at higher temperature, where the nitrate phase decomposes, liberating NOx that can be selectively converted to N_2 in the net reducing environment using conventional three-way catalyst formulations. Under these rich conditions, barium carbonate ($BaCO_3$) is stable, although the nitrate phase can displace either this phase or BaO under lean conditions [68,72]. Several studies have utilized diffuse reflectance FTIR to provide evidence of $Ba(NO_3)_2$ phase formation under lean conditions on the adsorber catalyst surface [4,68,71,73], although nitrite species have also been identified in the early stages of the NOx adsorption process [74]. Important challenges for research on these NOx adsorber catalyst materials are improving their overall durability, regeneration characteristics, and resistance to SO_2 poisoning.

It is clear that our high Na Pt/HTO:Si materials are fundamentally similar to NOx storage/adsorber catalysts in both chemical composition and functionality. One question that might be asked regarding the data shown in Figure 6 (comparing the ramp up and ramp down profiles for the high Na Pt/HTO:Si materials) is how the same material can both adsorb and desorb NOx over nearly the same temperature range (300-450°C). The answer is related to the different equilibrium catalyst surface conditions present as a result of the different dynamic test profiles. Mechanisms for NOx adsorption might involve the reaction of NO, NO_2, and O_2 with sodium hydroxide (NaOH), sodium bicarbonate ($NaHCO_3$), sodium carbonate (Na_2CO_3), or sodium oxide (Na_2O) to form stable sodium nitrite ($NaNO_2$) or $NaNO_3$ phases. Similar to other supported Pt catalysts, at temperatures beyond the temperature of maximum NOx conversion observed during a typical ramp up profile, the Pt surface is expected to be dominated by O atoms, resulting in an increased tendency to form NO_2 from NO [30,50,53]. In addition to the direct interaction with NO, both desorbed O atoms or NO_2 molecules can spill over to dispersed Na-containing phases near Pt particles, forming $NaNO_2$ and/or $NaNO_3$ phases.

Superimposed with this behavior is the fact that the $NaNO_2$/$NaNO_3$ phases melt and decompose at elevated temperatures, resulting in the release of NOx. Handbook data reports that bulk $NaNO_2$ and bulk $NaNO_3$ both melt prior to decomposition, with the onset of decomposition as low as 320 and 380°C, respectively [75]. Practically, however, much higher temperatures are required to achieve significant decomposition rates for bulk $NaNO_3$ (> 600°C), with $NaNO_2$ being an intermediate species in the decomposition process [76-78]. Previous work has shown that physical mixtures of $NaNO_3$ with SiO_2, TiO_2, or other oxides resulted in the accelerated decomposition of $NaNO_3$ (relative to bulk $NaNO_3$), due to significant interactions via solid state reactions or with acid sites on the oxide surfaces [78]. Thermogravimetric analysis (TGA) results in our lab (not shown) support these previous results; in a flowing air atmosphere using a 5°C/min heating rate, near complete decomposition of 12.9 wt.% $NaNO_3$ (3.5 wt.% Na) supported on a calcined HTO:Si support was achieved at ~550°C relative to ~800°C for a bulk $NaNO_3$ sample. The observed results for the ramp up profile, where NOx begins desorbing from the high Na Pt/HTO:Si material at ~300°C are consistent with these TGA results. Decomposition of the $NaNO_2$/$NaNO_3$ phases on actual catalyst samples appears to be complete by 500°C as the NOx conversion profile returns to approximately the 0% conversion baseline (see Figure 6). Because of the thermodynamic equilibrium between $NaNO_2$ and $NaNO_3$, there is a definite possibility of interconversion between these phases, depending on the exact atmosphere (O_2 content) and temperature conditions. From a performance standpoint, the exact identification and or distribution of the $NaNO_2$ and $NaNO_3$ phases in the catalyst material makes little difference since both of these phases result from NOx storage.

For the ramp down profile, which begins at high temperature (500°C) after a N_2 purge, the catalyst surface would be expected to be relatively clean with respect to $NaNO_2$, $NaNO_3$, or $NaHCO_3$. From the ramp up profile experiments, it is known that little or no NOx conversion or adsorption occurs at this temperature. The dispersed Na-containing phase in the high Na Pt/HTO:Si catalyst would be expected to be free of adsorbed NO or

NO_2 as well. However, as temperature is lowered to the point where $NaNO_2/NaNO_3$ phase decomposition becomes less favorable, storage of NOx can occur. Measurable NOx storage appears to take place over the temperature range of 450°C to ~275°C. Significant NOx conversion would be expected between nominally 200-275°C. As temperature further decreases during the ramp down test profile to < 200°C, where hydrocarbon oxidation is less facile, it is possible that the stored NOx species can more directly interact with the available hydrocarbons (C_3H_6) to facilitate NOx reduction.

Na contents intermediate between the low and high Na levels in the Pt/HTO:Si catalysts were also briefly examined as part of this study. For nominal 1 wt.% Pt/HTO:Si catalysts, Na contents between 1-2 wt.% were found to result in similar NOx adsorption and desorption behavior. Results similar to those shown in Figure 6 were reproduced in these cases, although several differences were noted. First, the magnitude of the NOx desorption peak during the ramp up test profile was considerably smaller than that obtained for higher Na contents. Second, the ramp down profile yielded a narrower temperature window of appreciable NOx conversion. Both of these observations are consistent with the lower Na levels in these samples relative to the high Na Pt/HTO:Si catalysts. HTO:Si materials with various Na contents (but containing no Pt) were also evaluated as control samples; these samples showed no appreciable NOx conversion or adsorption. This provides possible evidence for the lack of direct NO adsorption to produce $NaNO_2$, although additional experiments would be required to confirm this result.

In an effort to quantify the NOx adsorption capacity of the high Na Pt/HTO:Si catalyst material, several controlled experiments were performed. First, a high Na (3.32 wt.%) 0.94 wt.% Pt/HTO:Si catalyst was held for an extended time (2 h) under reaction conditions at 275°C. The observed steady state conversions under these conditions were 12%, 100%, 100%, and 0% for NOx, CO, C_3H_6, and C_3H_8, respectively. These values are consistent with those obtained in other isothermal tests of high Na Pt/HTO:Si materials (see Figure 7). Following this experiment, the catalyst was heated in 5% O_2 in N_2 to 500°C, held for 30 min to desorb all stored NOx species, and then cooled to 275°C. Significant NOx adsorption would be expected at this temperature based on previous ramp down tests with similar materials (see Figure 5). Then, to monitor the uptake of NO, a feed consisting of 305 ppm NO, 5% O_2, and balance N_2 was passed over the catalyst for 3 h, while the catalyst was maintained at 275°C. Integration of the NOx concentration profile over the 3 h time period yielded a total NOx uptake of ~2.0 cc (STP) per g of catalyst (~3 mg NO per g of catalyst). This corresponds to only a small fraction (~6%) of the Na in the catalyst formulation being converted to $NaNO_2/NaNO_3$. Possible reasons for the relatively inefficient utilization of the Na phase for NOx storage include poor dispersion of the Pt particles (resulting in poor NO oxidation activity), poor dispersion of the Na phase with respect to the Pt particles, and competition between $NaNO_2/NaNO_3$ phase formation and pre-existing (or in situ formed) $NaHCO_3$ or Na_2CO_3 phases.

Diffuse reflectance FTIR evaluation of the high Na Pt/HTO:Si catalyst sample was performed after its removal from the test unit following the NOx adsorption experiment. The spectra from this sample was compared to several other catalyst and control samples, including an identical high Na Pt/HTO:Si sample in as-calcined form, a fully acidified (Na content of 0.31 wt.%) and calcined HTO:Si support, and controlled $NaNO_2$ or $NaNO_3$ additions (equivalent to 3.5 wt.% Na in the high Na Pt/HTO:Si catalyst) via incipient wetness impregnation to the same calcined HTO:Si support sample. These latter samples were evaluated in a dried (100°C) but uncalcined form to preserve the nitrite or nitrate phases for subsequent analysis.

The FTIR spectra for the various samples described above are shown in Figure 8. All of the spectra showed a broad band at ~1640 cm^{-1} associated with the HTO:Si support. Specifically, this band can be assigned to a bending mode for water molecules coordinated to surface Ti^{+4} cations [79-81]. Control samples prepared using either $NaNO_2$ or $NaNO_3$ dispersed on the HTO:Si support contained a broad band in the 1325-1425 cm^{-1} region; the only possible distinguishing feature between the two species being a shoulder at ~1475 cm^{-1} associated with this band for the $NaNO_3$/HTO:Si sample. These results are consistent with a recent review of the identification of N_xO_y species by IR spectroscopy, which notes the difficulty in distinguishing between nitrate (NO_3^-) and nitrite (NO_2^-) surface species [82]. For the as-calcined high Na Pt/HTO:Si sample, no evidence of a significant $NaNO_2$/$NaNO_3$ band in this region exists. In contrast, the high Na Pt/HTO:Si sample examined after the NOx uptake experiment showed a definite broad band at ~1375 cm^{-1}, similar to the control samples. We believe that this is solid evidence for the existence of stable $NaNO_2$/$NaNO_3$ species in the high Na Pt/HTO:Si sample following the NOx uptake experiment. Analysis of the difference spectra between the high Na Pt/HTO:Si sample examined after the NOx uptake experiment and the as-calcined high Na Pt/HTO:Si sample showed a clear band at ~1400 cm^{-1} (see Figure 8, spectrum c). Several previous studies have assigned bands in the 1380-1415 cm^{-1} region to free nitrate or $NaNO_3$ species, consistent with our findings [82-87]. The existence of both $NaNO_2$ and $NaNO_3$ species in Na-promoted Pt/Al_2O_3 catalysts under reaction conditions (NO reduction by C_3H_6 in the absence of O_2) has been demonstrated by Yentekakis, et al. using x-ray photoelectron spectroscopy [88].

A few previous studies have examined the effect of Na (or other alkali metal) on supported noble metal catalysts for automotive catalyst applications. Interpretation of these literature results is complicated by the fact that different catalyst compositions (Pt, Pd, Rh, Ir, etc.) and reaction conditions (lean-burn vs. stoichiometric vs. simplified model reactions) have been used in these studies. These complicating factors make it difficult to generalize conclusions regarding the effect of alkali additions on catalyst performance.

In contrast to our work, Konsolakis, et al. observed a strong promoting effect of Na in Pt/Al_2O_3 catalysts (optimal Na loading of ~4.2 wt.%) used for NO reduction by CO and C_3H_6 in simulated exhaust gas under stoichiometric conditions (0.8% O_2) [89]. They proposed a specific model to explain this promotion, in which Na increases the strength of the Pt-NO chemisorption bond while weakening the N-O bond, therefore facilitating

NO dissociation on the reduced Pt surface. In addition to promoting increased conversion (of NO, CO, and C_3H_6) at a given temperature, significant increases in N_2 selectivity were observed. However, recent work on SCR of NOx via C_3H_6 under lean-burn conditions (8% O_2) using Ir black catalysts suggests that the primary effect of Na additions is to shift both the NOx and C_3H_6 conversion profiles to higher temperature [90]. This is consistent with fundamental work on the electrochemical promotion of Pt/Al_2O_3 for C_3H_6 oxidation, where higher O_2/C_3H_6 ratios resulted in Na additions yielding a lower benefit [91]. These latter observations are more consistent with our results, where Na additions to Pt/HTO:Si catalysts were found to delay catalyst light-off and lower NOx conversion efficiency for simulated lean-burn gasoline exhaust environments (8% O_2).

Burch and Watling showed that a 2.4 wt.% K_2O addition to a 1.0 wt.% Pt/Al_2O_3 catalyst used for lean-burn (5% O_2) NOx reduction via C_3H_6 (ramp up temperature profile) resulted in a decrease in maximum NOx conversion, a slight downward shift in the temperature of maximum NOx conversion, and a slight broadening of the temperature window of appreciable NOx conversion [92]. A 7.25 wt.% Cs_2O addition was shown to decrease maximum NOx conversion, shift the temperature of maximum NOx conversion slightly upward, and slightly broaden the temperature window of appreciable NOx conversion. These alkali metal oxide concentrations are equivalent to a 1.2 wt.% Na loading in the final catalyst, lower than the quantities typically present in high Na Pt/HTO:Si catalysts (3-5 wt.%). It is difficult to compare our experimental results to the above results because ramp up test profile tests with our materials proved to be the least reproducible in terms of quantifying NOx conversion and adsorption effects. Nonetheless, the lack of a significant positive benefit associated with alkali additions is consistent with other recent active lean-NOx catalysis results.

Recently, Cho and Gardner performed a study related to the steady state and transient testing of low and high Na Pt/HTO:Si catalysts for active lean-NOx applications [29]. Using a simpler simulated lean-burn exhaust feed with C_2H_4 as the hydrocarbon reductant, it was found that the effect of Na can be beneficial or detrimental depending on the HC:NOx ratio and the temperature range of interest. For high Na Pt/HTO:Si catalysts run at steady state test conditions with low HC:NOx ratios (2:1), Na inhibits NOx reduction activity at low temperature (< 300°C), while enhancing it at higher temperature (> 300°C). At higher HC:NOx ratios (6:1), the behavior is more complex; an improvement in NOx reduction activity is observed in the low temperature regime at the expense of high temperature activity. Under these conditions, high Na was found to inhibit NOx conversion performance over the entire temperature range, with a very slight shift in light-off toward higher temperature – results that are consistent with our steady state test results (see Figure 7). A dual bed staged reactor configuration with a high Na Pt/HTO:Si catalyst placed upstream of a low Na Pt/HTO:Si catalyst was found to broaden the overall temperature window of NOx conversion, improving overall lean-NOx catalyst performance. Transient experiments utilizing rich and lean half-cycles were also performed that showed a significant benefit of high Na Pt/HTO:Si catalysts. It was proposed that the multifunctional nature of the high Na Pt/HTO:Si catalyst includes both electron donation effects and NOx storage capability. In addition to the electron donation

effects described by Konsolakis, et al. [89], it was hypothesized that similar phenomena could lead to weakened hydrocarbon adsorption on Pt, resulting in inhibited hydrocarbon oxidation and improved NOx conversion [93]. At least one other study has also noted an inverse correlation between additive basicity and hydrocarbon oxidation activity [4].

Similar effects were observed in the case of high K Pt/HTO:Si catalysts synthesized as part of this study, either via residual (unexchanged) K^+ levels, or via addition of a potassium nitrate (KNO_3) precursor via incipient wetness impregnation of a low Na Pt/HTO:Si catalyst followed by drying and calcination. Results nearly identical to those shown in Figures 4 and 7 for both low and high Na Pt/HTO:Si materials were observed for low and high K Pt/HTO:Si materials in either a ramp down or isothermal test mode, respectively.

Comparison to Other Supported Pt Catalysts

Figure 9 shows NOx conversion profile data for nominal 1.0 wt.% Pt catalysts supported on TiO_2 and SiO_2, as well as Pt/Al_2O_3 and Pt/ZSM-5 benchmark catalysts with similar Pt loading obtained from a catalyst supplier. A separate low Na Pt/HTO:Si catalyst from that described above (see Figures 1 and 2) was used as a control sample to compare to the other supported Pt catalysts shown in Figure 9. The similar NOx conversion profile and maximum NOx conversion (73% vs. 68%) of these two low Na Pt/HTO:Si catalysts demonstrate the excellent reproducibility of Pt/HTO:Si catalyst preparation (Na levels: 0.04 % vs. 0.11%, Pt Levels: 1.12 % vs. 1.18 %). Data for a low Na Pt/HTO catalyst are also shown in Figure 9 for comparison.

The data for all the catalysts shown in Figure 9 are quite similar. The Pt/SiO_2 and Pt/ZSM-5 catalysts have slightly higher (although probably not statistically significant) maximum NOx conversion and a lower light-off temperature than the other catalyst formulations. However, considerable previous work has demonstrated that Pt/ZSM-5 catalysts exhibit significant deactivation during aging in environments containing steam [11,94]. SiO_2 is also known to be sensitive to surface area loss in hydrothermal environments. The other four catalysts (Pt/HTO:Si, Pt/HTO, Pt/TiO_2, and Pt/Al_2O_3) appear to have similar performance, although the Pt/HTO:Si catalyst may be slightly superior to the Pt/TiO_2 catalyst, perhaps due to the higher surface area of the HTO:Si support and/or the benefits of ion exchange vs. incipient wetness impregnation preparation. Several previous studies have shown similar trends for SiO_2-supported Pt catalysts relative to Al_2O_3-supported Pt catalysts [9]. Not shown in Figure 9 is the fact that the conversion profiles for CO, C_3H_6, and C_3H_8 were very similar for all of the catalysts. These results provided motivation for characterization of HTO- and HTO:Si-supported Pt catalysts relative to the conventional catalysts, as well as further investigation of these novel catalysts in coated form for monolith applications.

Various techniques were used to characterize the various supported Pt catalysts examined in this study. These catalysts were characterized in the as-calcined form (600°C/2h/air) unless otherwise indicated. Representative materials were selected with respect to the different classes of supported Pt catalysts evaluated within this work. Catalyst

preparation details, composition, and a summary of physical characterization data (BET surface area and H_2 chemisorption) for these materials are shown in Table 1.

The physical properties summarized in Table 1 give an indication of the high surface areas achievable with HTO:Si-supported catalysts. Low Na Pt/HTO:Si catalysts exhibit BET surface areas greater than 100 m^2/g, pore volumes of ~0.4 cc/g, and relatively small average pore sizes (~12 nm in diameter). Note that the amount and dispersion of Pt has little influence on these overall characteristics; the values shown in Table 1 for the low Na Pt/HTO:Si material are very similar to those obtained with a fully acidified HTO:Si material containing no added Pt (denoted as H^+ Form HTO:Si) [11]. These values are significant improvements upon those observed with low Na Pt/HTO catalysts, as well as Degussa P25 TiO_2-supported Pt, and competitive with other high surface area conventional oxide or zeolite-supported Pt catalysts (see Table 1). These improvements indicate the important role that SiO_2 doping plays in imparting increased thermal stability to the HTO:Si support. The main role of SiO_2 doping is to retard the high temperature anatase to rutile phase transformation, which is largely responsible for significant deterioration of the physical properties of TiO_2 supports at high temperatures [11,95-98]. This result was verified by x-ray diffraction (not shown).

The presence of significant quantities of Na in the Pt/HTO:Si catalysts was found to alter the observed physical characteristics, generally resulting in lower surface area and pore volume, along with increased pore size. These values were still somewhat of an improvement with respect to Pt/HTO or Pt/TiO_2 catalysts. The surface area of the Na^+ form of the HTO:Si support was significantly lower than that observed for the corresponding Na free (fully acidified) H^+ Form HTO:Si material [15,99]. This deterioration in properties has been correlated with mixed oxide (Na-Ti-O or Na-Ti-Si-O) phase formation at elevated temperatures (> 400°C) [15,100]. The Na levels in the high Na Pt/HTO:Si catalysts correspond to ~50% of the Na content in the original Na form HTO:Si support. X-ray diffraction studies on these catalyst materials, as well as nominally 50% acidified Na form HTO:Si supports, did not show direct evidence for mixed oxide phase formation. This might be due to the decreased amount of crystalline mixed oxide phase(s) formed in these samples, or possibly the formation of less crystalline mixed oxide precursor phases. Nevertheless, the Na content correlates well with the observed physical characteristics; the high Na Pt/HTO:Si catalyst data lies intermediate between the data observed previously for the original Na^+ form HTO:Si support and the low Na Pt/HTO:Si catalyst. No significant differences were observed in the x-ray diffraction patterns of low and high Na Pt/HTO:Si catalysts (not shown).

H_2 chemisorption results for the various supported Pt catalysts are also shown in Table 1. Following the standard calcination pretreatment (600°C/2h/air), the catalyst samples were reduced in flowing H_2 at 400°C for 2h prior to chemisorption measurements. Following these pretreatment procedures the dispersions measured for the various HTO- and HTO:Si-supported Pt catalysts were quite low, ranging from 4-10%. A range of reduction temperatures was investigated for these samples to investigate the possible role of strong metal support interaction (SMSI) phenomena affecting the H_2 chemisorption

measurements [101,102]. As the reduction temperature was increased from 150 to 400°C, Pt dispersion continued to increase for the Pt/HTO:Si sample. This indicated that SMSI phenomena did affect H_2 chemisorption measurements; in fact, higher reduction temperatures were required to optimize Pt dispersion in these samples via restructuring/redispersion of Pt particles following the initial 600°C calcination procedure [102,103]. Calculated average Pt particle sizes (assuming spherical particles) corresponding to these measured dispersions ranged from approximately 10-30 nm in diameter.

Only the Pt/Al_2O_3 catalyst had a significantly better Pt dispersion than the HTO- or HTO:Si-supported Pt catalysts. The TiO_2-, SiO_2-, and ZSM-5-supported Pt catalysts had similar Pt dispersions relative to the Pt/HTO and Pt/HTO:Si materials. The low Pt dispersions observed for the majority of these samples is surprising given the wide range of surface areas of the various catalyst samples (see Table 1). The final Pt dispersion is apparently more directly influenced by the choice of catalyst precursor, specific support chemistry, and/or the aggressive calcination conditions used for catalyst pretreatment, which would be expected to promote sintering of Pt particles [102,103]. In the absence of initial calcination procedures, less aggressive hydrogen pretreatment of as-prepared HMO-supported noble metal catalysts has been shown to produce high dispersions, even at relatively high weight loadings [19]. However, these less aggressive pretreatment procedures are not appropriate for autmotive exhaust catalysts.

The similarity of the NOx reduction activity data shown in Figure 9 correlates well with the relatively small range of Pt dispersion (4-10%, see Table 1) for most of the various supported Pt catalysts. However, a substantial amount of previous work has noted the lack of significant Pt dispersion effects on active lean-NOx reduction activity [9,30,51], with SiO_2-supported catalysts possibly showing a slight dependence [9,35]. It is possible that the poor Pt dispersions observed for the high Na Pt/HTO:Si catalysts may be in part responsible for inefficient utilization of the Na-containing phase for NOx storage.

TEM evaluation of selected Pt/HTO and Pt/HTO:Si samples was also performed as part of the overall catalyst characterization efforts. Figure 10 is a composite of several photomicrographs showing the microstructure of the low Na Pt/HTO:Si catalyst imaged via TEM. This catalyst material consisted of large aggregates/agglomerates of very small individual particles. Imaging of individual Pt particles against the background of the HTO:Si support matrix was facilitated via removal of the objective aperture, which improved the contrast between the two distinct phases. In the various photomicrographs in Figure 10, the Pt phase is resolved as dark, equiaxed particles against the background of the fine-grained support matrix (TiO_2 particles). These Pt particles were positively identified by energy dispersive spectroscopy (EDS) analysis, and were found to be metallic in nature (verified by the lack of an oxygen peak in the EDS spectra). Pt particles with a wide variation in size (15-130 nm) were observed in this sample, illustrated by the various photomicrographs in Figure 10. Figure 10 (left) and Figure 10 (middle) show representative regions with small and intermediate size Pt particles, respectively. The larger size range Pt particles (see Figure 10, right) were often faceted,

and single crystals. Further TEM work using thin sections prepared from granulated catalyst powders verified the observed size range of Pt particles. However, this additional work showed that a high density of smaller (30-50 nm) Pt particles existed within TiO_2 aggregates/agglomerates relative to those located near the exterior of the TiO_2 aggregates/agglomerates (90-200 nm). Viewing conditions for non-thin section TEM powder specimens are likely biased toward observation of the exterior of TiO_2 aggregates/agglomerates. Anatase was identified as the predominant phase composing the HTO:Si support by electron diffraction (see inset electron diffraction pattern in Figure 10, right). Higher resolution TEM imaging showed that the individual anatase particles ranged in size from 4-8 nm.

Figure 11 shows the microstructure observed for the high Na Pt/HTO:Si catalyst sample via TEM. Relative to the low Na Pt/HTO:Si catalyst, it was very apparent that a lower number density of discrete, large (50-200 nm), faceted Pt particles were distributed throughout the support. These large Pt particles showed single crystal electron diffraction patterns, with the diffraction pattern shown in Figure 11 (inset) indicative of a [112] orientation of the face centered cubic Pt crystal structure. Higher resolution TEM imaging showed a similar distribution (relative to the low Na Pt/HTO:Si catalyst) of smaller (20-40 nm) and larger (80-150 nm) Pt particles between the interior and exterior of TiO_2 aggregates/agglomerates, respectively. Figure 12 shows the EDS analysis spectrum of an area of the support apparently devoid of Pt particles. This result showed the presence of Ti, O, and Si, consistent with the SiO_2-doped TiO_2 formulation of the HTO:Si support (5:1 Ti:Si ratio, ~87 wt.% TiO_2/13 wt.% SiO_2), as well as a small but consistent Na signal. Very similar spectra were obtained for the support phase in the low Na Pt/HTO:Si catalyst, with the exception of the Na peak.

The anion exchanged low Na Pt/HTO:Si catalyst sample (NOx reduction activity data shown in Figure 3) was also evaluated by TEM for comparison to the other HTO:Si-supported Pt catalysts. As illustrated by the various images in Figure 13, this Pt/HTO:Si catalyst also possessed a very wide range of Pt particle size (10 nm – 200 nm). Intermediate size Pt particles are shown in Figure 13 (left), with very large Pt particles shown in Figure 13 (middle). These large particles appeared to be bicrystals since it was difficult to obtain a single crystal electron diffraction pattern. Electron diffraction of the TiO_2 support phase showed results very similar to those shown in Figure 10 (right). No residual Cl^- was identified in the EDS spectra of either the support phase or the distinct Pt particles. The high magnification portion of Figure 13 (right) shows both the size of the smallest distinguishable Pt particles (~10 nm) as well as the fact that the particle size of the anatase support phase is approximately equal to that of the smallest Pt particles. Relative to the other HTO- or HTO:Si-supported Pt catalysts shown in Table 1, this particular sample showed the lowest dispersion (~4 %) as measured by H_2 chemisorption.

For pure HTO supports, fabricated without the addition of silica, dramatic microstructural changes are observed. This is illustrated by Figure 14, which shows the microstructure of the Pt/HTO sample. In this case, it was even more difficult to distinguish Pt particles from the crystalline TiO_2 support phase (also anatase as demonstrated by the electron

diffraction pattern shown in the inset to Figure 14 and by separate x-ray diffraction analysis). As with previous samples, EDS was often used to positively identify Pt particles with a range of particle sizes. In this case, the anatase support particles were larger in size (20-30 nm) and significantly more crystalline (as evidence by the sharper rings and the large number of spots in the inset electron diffraction pattern shown in Figure 14) than the anatase TiO_2 particles observed in the case of the HTO:Si support (see Figures 10-12). Pt particles observed were very large, ranging from 40 to greater than 100 nm in size, and appeared as single crystals, bicrystals, and twinned single crystals. These particle sizes are slightly larger than those observed for the low Na Pt/HTO:Si catalyst, consistent with the slightly lower metal dispersion determined for this sample via H_2 chemisorption (~6 %, see Table 1).

In all cases, the observed TEM results regarding Pt particle size for the HTO- and HTO:Si-supported catalysts are significantly larger than the average Pt particle sizes calculated from H_2 chemisorption measurements (10-30 nm). It should be noted that because of the lack of significant contrast difference between the Pt and anatase particles, it was extremely difficult to image discrete Pt particles which were comparable in size to (or smaller than) these individual anatase particles (4-8 nm). The presence of a substantial fraction of smaller, unresolvable Pt particles might explain the consistent discrepancy between the average Pt particle size calculated from H_2 chemisorption measurements and the observed TEM results. In an effort to further probe the possible presence of smaller Pt particles, additional high resolution TEM, as well as scanning transmission electron microscopy (STEM), were also performed; in both cases, definitive identification of Pt particles smaller than 30 nm was not successful. An alternate explanation involves the difference in the state of the catalyst between TEM examination (as-calcined or after activity testing) and H_2 chemisorption measurements. It is well recognized that the type of reduction treatment (400°C in flowing H_2) used as part of the H_2 chemisorption protocol could act to redisperse or restructure the Pt particles, resulting in a decrease in particle size relative to the same catalyst after treatment in an oxidizing environment (calcination, activity testing) [102,103]. Our TEM results for the Pt/HTO:Si catalysts are consistent with similar electron microscopy work performed by Cho and Gardner [29].

Summary

This report describes the development of bulk hydrous metal oxide (HMO)-supported Pt catalysts for lean-burn NOx catalyst applications. Specifically, HMO compositions based on hydrous titanium oxide (HTO) and silica-doped hydrous titanium oxide (HTO:Si) were evaluated. Anion and cation exchange methods were used to prepare nominal 1.0 wt.% Pt/HTO or Pt/HTO:Si catalysts. Catalyst activity results generally fell into two different categories, depending on the Na content of the Pt/HTO:Si catalysts. Pt/HTO:Si catalysts with low Na content (< 0.5 wt.%) were found to be very active for NOx reduction in simulated lean-burn exhaust environments utilizing propylene (C_3H_6) as the major reductant species. Similar NOx reduction performance was observed for these

materials using various test profiles (ramp up, ramp down, and isothermal). The activity and performance of these low Na Pt/HTO:Si catalysts were comparable to supported Pt catalysts prepared using conventional oxide or zeolite supports. High Na Pt/HTO:Si catalysts showed significantly different performance over the range of test profiles examined. In ramp down test conditions, Pt/HTO:Si catalysts with Na contents in the range of 3-5 wt.% showed a wide temperature window of appreciable NOx conversion relative to low Na Pt/HTO:Si catalysts. Similar results were obtained with high Na Pt/HTO:Si catalysts prepared using two different methods. Full reactant species analysis using both ramp up and isothermal test conditions with the high Na Pt/HTO:Si catalysts, as well as diffuse reflectance FTIR studies, showed that this phenomenon was related to transient NOx storage effects associated with $NaNO_2/NaNO_3$ formation. These nitrite/nitrate species were found to decompose and release NOx at temperatures above 300°C in the reaction environment (ramp up profile). A separate NOx uptake experiment at 275°C in $NO/N_2/O_2$ showed that the Na phase was inefficiently utilized for NOx storage. Steady state tests showed that the effect of the increased Na content was to delay NOx light-off and to decrease the maximum NOx conversion. Similar results were also observed for high K Pt/HTO:Si catalysts. Catalyst characterization studies showed that Pt/HTO:Si catalysts had high surface area relative to conventional TiO_2-supported catalysts, although high Na contents were detrimental to the physical properties of the HTO:Si support. Most supported Pt catalysts examined in this study had poor Pt dispersions (4-10%, as measured by H_2 chemisorption), although dispersion results did not directly correlate with NOx reduction activity. Microstructural characterization of the Pt/HTO:Si and Pt/HTO catalysts revealed the existence of a wide range of Pt particle sizes and the crystallization of the HTO or HTO:Si support into the anatase form of TiO_2 as a result of catalyst pretreatment (600°C/2h/air calcination). The overall results show the potential utility of these novel catalysts for lean-burn exhaust applications, particularly coated forms of the ion exchangeable HTO:Si support, which can be used to both disperse the active phase (Pt) and provide a residual alkali content (e.g., Na) to build a NOx storage functionality into the catalyst.

Acknowledgments

This work was supported by the United States Department of Energy under Contract DE-AC04-94AL85000. Sandia National Laboratories is a multiprogram laboratory operated by Sandia Corporation, a Lockheed Martin Company, for the United States Department of Energy. This project was specifically supported with funds from the Office of Advanced Automotive Technologies within the Office of Transportation Technologies in DOE/EE. This work was the result of a Cooperative Research and Development Agreement (CRADA) between Sandia National Laboratories and the Low Emission Technologies Research and Development Partnership (LEP). The authors would like to acknowledge the support that the staff at General Motors Corporation, Ford Motor Company, and DaimlerChrysler Corporation have given to us to ensure that this project would be a technical success. We are also indebted to our former Sandia team members, Stephen E. Lott, Steven J. Lockwood, Charlene A. Matlock, and John B. Oelfke, for their dedication

to this project. The efforts of Thomas J. Headley at Sandia and Karren L. More at Oak Ridge National Laboratory in providing high quality electron microscopy of various catalyst samples are deeply appreciated. Finally, the efforts of Jason E. Mudd at Sandia in assisting in various catalyst characterization activities are acknowledged.

References

1. M. P. Walsh, SAE Technical Paper 1999-01-0107 (1999).
2. H. Luders, P. Stommel, and S. Geckler, SAE Technical Paper 1999-01-0108 (1999).
3. W. Bogner, M. Kramer, B. Krutzsch, S. Pischinger, D. Voigtlander, G. Wenninger, F. Wirbeleit, M. S. Brogan, R. J. Brisley, and D. E. Webster, Appl. Catal. B 7 (1995) 153.
4. N. Takahashi, H. Shinjoh, T. Iijima, T. Suzuki, K. Yamazaki, K. Yokota, H. Suzuki, N. Miyoshi, S. Matsumoto, T. Tanizawa, T. Tanaka, S. Tateishi, and K. Kasahara, Catal. Today 27 (1996) 63.
5. J. Hoard, SAE Technical Paper 2001-01-0185 (2001).
6. B. H. Engler, J. Leyrer, E. S. Lox, and K. Osgathe, SAE Technical Paper 930735 (1995).
7. A. Obuchi, A. Ohi, M. Nakamura, A. Ogata, K. Mizuno, and H. Ohuchi, Appl. Catal. B 2 (1993) 71.
8. H. Hamada, Catal. Today 22 (1994) 21.
9. R. Burch and P. J. Millington, Catal. Today 26 (1995) 185.
10. R. Burch and P. J. Millington, Catal. Today 29 (1996) 37.
11. S. E. Lott, T. J. Gardner, and L. I. McLaughlin, Sandia Report, SAND96-2267, Sandia National Laboratories, Albuquerque, NM (1996).
12. H. Klein, S. Lopp, and E. Lox, SAE Technical Paper 1999-01-0109 (1999).
13. A. Ruvarac, in "Inorganic Ion Exchange Materials" (Ed. A. Clearfield), CRC press, Boca Raton, 1982, p. 141.
14. M. Abe, in "Inorganic Ion Exchange Materials" (Ed. A. Clearfield), CRC press, Boca Raton, 1982, p. 161.
15. R. G. Dosch, H. P. Stephens, F. V. Stohl, C. H. F. Peden, and B. C. Bunker, Sandia Technical Report, SAND89-2399, Sandia National Laboratories, Albuquerque, NM (1990).
16. R. G. Dosch, H. P. Stephens, and F. V. Stohl, Sandia Technical Report, SAND89-2400, Sandia National Laboratories, Albuquerque, NM (1990).
17. R. G. Dosch and L. I. McLaughlin, Sandia Technical Report, SAND92-0388, Sandia National Laboratories, Albuquerque, NM (1992).
18. T. J. Gardner and L. I. McLaughlin, Mat. Res. Soc. Symp. Proc. 432 (1997) 249.
19. T. J. Gardner, L. I. McLaughlin, L. R. Evans, and A. K. Datye, Stud. Surf. Sci. Catal. 118 (1998) 245.
20. R. G. Dosch and H. P. Stephens, US Patent 5 461 022 (1995), to Sandia National Laboratories.

21. S. E. Lott, T. J. Gardner, L. I. McLaughlin, C. A. Matlock, and J. B. Oelfke, US Patent 5 795 553 (1998), to Low Emission Technologies Research and Development Partnership.
22. T. J. Gardner, S. E. Lott, S. J. Lockwood, and L. I. McLaughlin, US Patent No. 5 830 421 (1998), to Low Emission Technologies Research and Development Partnership.
23. T. J. Gardner, S. E. Lott, S. J. Lockwood, and L. I. McLaughlin, US Patent No. 6 165 934 (2000), to Low Emission Technologies Research and Development Partnership.
24. H. P. Stephens, R. G. Dosch, and F. V. Stohl, Ind. Eng. Chem. 24 (1985), 15.
25. H. P. Stephens and R. G. Dosch, Stud. Surf. Sci. Catal. 31 (1987) 271.
26. T. J. Gardner, L. I. McLaughlin, and R. S. Sandoval, Prepr. Fuels Div., Amer. Chem. Soc. 41 (1996) 1008.
27. S. E. Lott, T. J. Gardner, L. I. McLaughlin, and J. B. Oelfke, Fuel, 75 (1996), 1457.
28. A. V. Cugini, D. Krastman, R. L. Thompson, M. V. Ciocco, and T. J. Gardner, Catal. Today, 43 (1998) 291.
29. B. K. Cho and T. J. Gardner, Submitted to Appl. Catal. B.
30. R. Burch, P. J. Millington, and A. P. Walker, Appl. Catal. B 4 (1994) 65.
31. A. Obuchi, A. Ogata, H. Takahashi, J. Oi, G. R. Bamwenda, and K. Mizuno, Catal. Today 29 (1996) 103.
32. A. Obuchi, I. Kaneko, J. Oi, A. Ohi, A. Ogata, G. R. Bamwenda, and S. Kushiyama, Catal. Today 15 (1998) 37.
33. B. K. Cho, J. Catal. 142 (1993) 418.
34. B. K. Cho and J. Yie, Appl. Catal. B 10 (1996) 263.
35. F. Jayat, C. Lembacher, U. Schubert, and J. A. Martens, Appl. Catal. B 21 (1999) 221.
36. B. H. Engler, J. Leyrer, E. S. Lox, and K. Ostgathe, Stud. Surf. Sci. Catal. 96 (1995) 529.
37. J. S. Feeley, M. Deeba, and R. J. Farrauto, SAE Technical Paper 950747 (1995).
38. K. M. Adams, J. V. Cavataio, and R. H. Hammerle, Appl. Catal. B 10 (1996) 157.
39. K. C. C. Kharas, M. J. Miller, and J.-Y. Yan, SAE Technical Paper 982604 (1998).
40. P. Ciambelli, P. Corbo, and F. Migliardini, Catal. Today 59 (2000) 279.
41. T. Tanaka, T. Okuhara, and M. Misono, Appl. Catal. B 4 (1994) L1.
42. R. Burch and T. C. Watling, J. Catal. 169 (1997) 45.
43. R. Burch, P. Fornasiero, and T. C. Watling, J. Catal. 176 (1998) 204.
44. M. Sasaki, H. Hamada, Y. Kintaichi, and T. Ito, Catal. Lett. 15 (1992) 297.
45. C. Rottlander, R. Andorf, C. Plog, B. Krutzsch, and M. Baerns, Appl. Catal. B 11 (1996) 49.
46. G. R. Bamwnda, A. Obuchi, A. Ogata, and K. Mizuno, Chem. Lett. (1994) 2109.
47. T. Okuhara, Y. Hasada, and M. Misono, Catal. Today 35 (1997) 83.
48. D. K. Captain and M. D. Amiridis, J. Catal. 184 (1999) 377.
49. D. K. Captain and M. D. Amiridis, J. Catal. 194 (2000) 222.
50. R. Burch and T. C. Watling, Catal. Lett. 43(1997) 19.

51. J. A. A. van den Tillart, J. Leyrer, S. Eckhoff, and E. S. Lox, Appl. Catal. B 10 (1996) 53.
52. R. Burch and J. A. Sullivan, J. Catal. 182 (1999) 489.
53. E. Xue, K. Seshan, and J. R. H. Ross, Appl. Catal. B 11 (1996) 65.
54. K. C. Taylor, Cat. Rev. Sci. Eng. 35 (1993) 457.
55. F. Acke and M Skoglundh, Appl. Catal. B 22 (1999) L1.
56. M. Inaba, Y. Kintaichi, and H. Hamada, Catal. Lett. 36 (1996) 223.
57. Z. Liu, J. Tabora, and R. J. Davis, J. Catal. 149 (1994) 117.
58. M. Itoh, H. Hattori, and K. Tanabe, J. Catal. 35 (1974) 225.
59. J. R. Sohn, H. J. Jang, M. Y. Park, E. H. Park, and S. E. Park, J. Mol. Catal. 93 (1994) 149.
60. P. K. Doolin, S. Alerasool, D. J. Zalewski, and J. F. Hoffman, Catal. Lett. 25 (1994) 209.
61. E. I. Ko, J. P. Chen, and J. G. Weissman, J. Catal. 105 (1987) 511.
62. K. M. Adams, J. V. Cavataio, T. Sale, W. A.. Rimkus, and R. H. Hammerle, SAE Technical Paper 962049 (1996).
63. M. Deeba, J. Feeley, R. J. Farrauto, N. Steinbock, and A. Punke, SAE Technical Paper 952491 (1995).
64. J. Leyrer, E. S. Lox, K. Ostgathe, W. Strehlau, T. Kreuzer, and G. Garr, SAE Technical Paper 960133 (1996).
65. C.R. Narayanan, S. Srinivasan, A. K. Datye, R. Gorte, and A. Biaglow, J. Catal. 138 (1992) 659.
66. S. Srinivasan, C.R. Narayanan, A. Biaglow, R. Gorte, and A. K. Datye, Appl. Catal. A 132 (1995) 271.
67. S. Srinivasan, C.R. Narayanan, and A. K. Datye, Appl. Catal. A 132 (1995) 289.
68. T. Kobayashi, T. Yamada, and K. Kayano, SAE Technical Paper 970745 (1997).
69. L. Olsson, H. Persson, E. Fridell, M. Skoglundh, and B. Andersson, J. Phys. Chem. B. 105 (2001) 6895.
70. E. Fridell, H. Persson, B. Westerberg, L. Olssen, and M. Skoglundh, Catal. Lett. 66 (2000) 71.
71. H. Mahzoul, J. F. Brilhac, and P. Gilot, Appl. Catal. B. 20 (1999) 47.
72. S. Balcon, C. Potvin, L. Salin, J. F. Tempere, and G. Djega-Mariadassou, Catal. Lett. 60 (1999) 39.
73. E. Fridell, M. Skoglundh, B. Westerberg, S. Johansson, and G. Smedler, J. Catal. 183 (1999) 196.
74. H. Y. Huang, R. Q. Long, and R. T. Yang, Energy and Fuels 15 (2001) 205.
75. R. C. Weast (Ed.), CRC Handbook of Chemistry and Physics, CRC Press, Boca Raton (1983) p. B-141.
76. E. S. Freeman, J. Phys. Chem. 60 (1956) 1487.
77. B. D. Bond and P. W. M. Jacobs, J. Chem. Soc. A. Inorg. Phys. Theor. (1966) 1265.
78. Y. Hoshino, T. Utsunomiya, and O. Abe, Bull. Chem. Soc. Jpn. 54 (1981) 1385.
79. L. Shao, L. Zhang, M. Chen, H. Lu, and M. Zhou, Chem Phys. Lett. 343 (2001) 178.

80. G. Marta, S. Coluccia, L. Marchese, V. Augugliaro, V. Loddo, L. Palmisano, and M. Schiavello, Catal. Today 53 (1999) 695.
81. V. Augugliaro, S. Coluccia, L. Marchese, G. Martra, L. Palmisano, and M. Schiavello, Appl. Catal. B. 20 (1999) 15.
82. K. I. Hadjiivanov, Catal. Rev. – Sci. Eng. 42 (2000) 71.
83. K. Nakamoto, Infrared and Raman Spectra of Inorganic and Coordination Compounds. Part A. Theory and Applications in Inorganic Chemistry, John Wiley and Sons, New York, 1997.
84. E. Ivanova, K. Hadjiivanov, D. Klissurski, M. Bevilacqua, T. Armaroli, and G. Busca, Microporous and Mesoporous Mater. 46 (2001) 299.
85. O. Monticelli, R. Loenders, P. A. Jacobs, and J. A. Martens, Appl. Catal. B. 21 (1999) 215.
86. A. Satsuma, K. Yamada, K. Sato, K. Shimizu, T. Hattori, and Y. Murakami, Catal. Lett. 45 (1997) 267.
87. C. C. Addison and B. M. Gatehouse, J. Chem. Soc. (1960) 613.
88. I. V. Yentekakis, A. Palermo, N. C. Filkin, M. S. Tikhov, and R. M. Lambert, J. Phys. Chem. B 101 (1997) 3759.
89. M. Konsolakis, N. Macleod, J. Isaac, I. V. Yentekakis, and R. M. Lambert, J. Catal. 193 (2000) 330.
90. C. Wogerbauer, M. Maciejewski, M. M. Schubert, and A. Baiker, Catal. Lett. 74 (2001) 1.
91. N. C. Filkin, M. S. Tikhov, A. Palermo, and R. M. Lambert, J. Phys. Chem. A 103 (1999) 2680.
92. R. Burch and T. C. Watling, Appl. Catal. B 11 (1997) 207.
93. N. D. Lang, S. Holloway, and J. K. Norskov, Surf. Sci. 150 (1985) 24.
94. K. C. C. Kharas, H. J. Robota, and D.-J. Liu, and A. K. Datye, Prepr. Am. Chem. Soc., Fuel Chem. Div. 40 (1995) 1068.
95. J. R. Sohn, H. J. Jang, M. Y. Park, E. H. Park, and S. E. J. Park, J. Mol. Catal. 93 (1994) 149.
96. P. K. Doolin, S. Alerasool, D. J. Zalewski, and J. F. Hoffman, Catal. Lett. 25 (1994) 209.
97. Y. Suyama and A. Kato, Yogyo-Kyokai-Shi 86 (1978) 119.
98. C. U. I. Odenbrand, S. L. T. Andersson, L. A. H. Andersson, J. G. M. Brandin, and G. Busca, J. Catal. 125 (1990) 541.
99. T. J. Gardner, L. I. McLaughlin, and D. L. Mowery, unpublished work.
100. S. Peercy, R. G. Dosch, and B. Morosin, Sandia Report, SAND76-0556, Sandia National Laboratories, Albuquerque, NM (1977).
101. G. L. Haller and D. E. Resasco, Adv. Catal. 36 (1989) 173.
102. S. A. Stevenson, J. A. Dumesic, R. T. K. Baker, and E. Ruckenstein (eds.), Metal-Support Interactions in Catalysis, Sintering, and Redispersion, Van Nostrand Rheinhold, New York, 1987.
103. C. H. Bartholomew, in Catalysis, Volume 10, (J. J. Spivey and S. K. Agarwal, eds.), Royal Society of Chemistry, Cambridge (1993) 41.

Table 1. Catalyst Description, Composition, and Characterization Data

Catalyst Description	**Wt.% Pt^**	**Wt.% Na^**	**Physical Properties+**	**% Pt Dispersion***
Na^+ Form HTO:Si	NA	10.28	46.4/0.36/30.8	NA
H^+ Form HTO:Si	NA	0.31	153.8/0.49/12.9	NA
Pt/HTO:Si – Anion Exchange	0.95	0.01	110.6/0.31/11.1	4.2
Low Na Pt/HTO:Si – Cation Exchange + Acidification	1.10	0.22	135.2/0.42/12.5	8.2
Low Na Pt/HTO – Cation Exchange + Acidification	1.11	0.10	38.5/0.37/38.1	5.5
High Na Pt/HTO:Si – Cation Exchange	1.03	3.84	84.9/0.34/18.0	8.3
Pt/Al_2O_3	1.0	NA	145.6/0.52/14.3	26.6
Pt/SiO_2	1.0	NA	264.3/1.42/21.4	8.1
Pt/TiO_2	1.0	NA	34.2/0.34/40.0	4.6
Pt/ZSM-5	1.0	NA	369.0/0.23/2.5	5.6

^ Metal and Na concentrations are reported on a calcined weight basis.

+ Denotes surface area (m^2/g)/total pore volume (cc/g)/average pore diameter (nm)

* Dispersion values calculated from monolayer capacity extrapolated to zero pressure (determined from total H_2 uptake) and total Pt concentration in sample as measured by AAS. Value represents the average of at least two measurements or samples where possible.

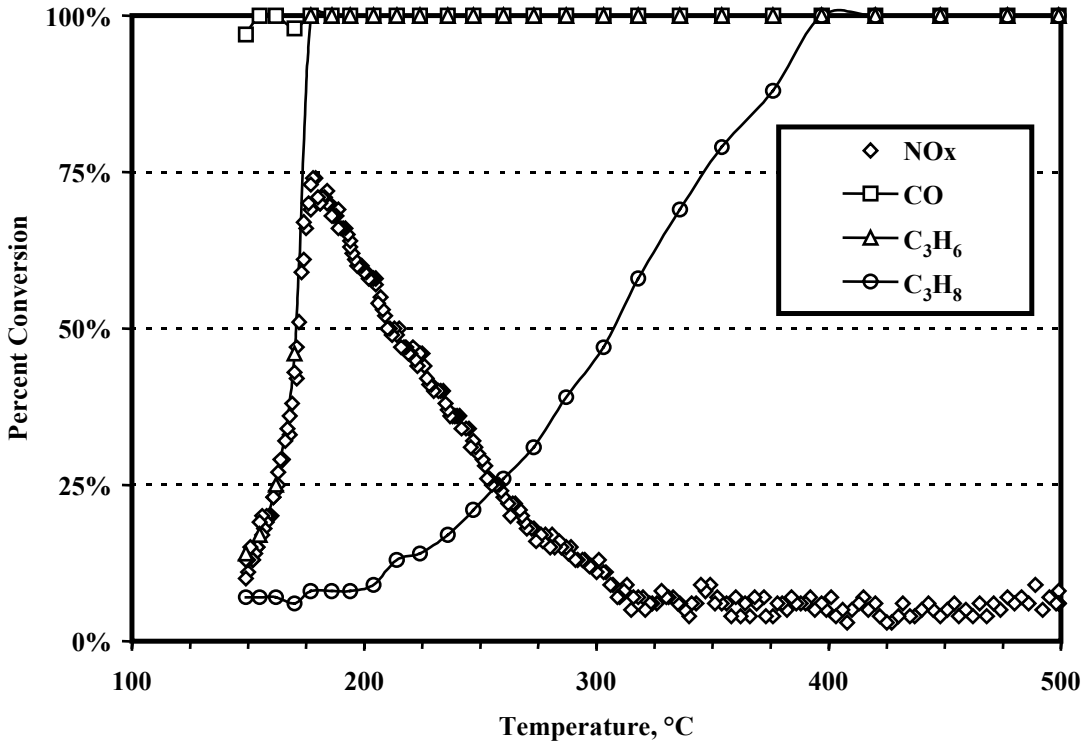

Figure 1. Conversion profiles for all species (CO, C_3H_6, C_3H_8, and NOx) for a low Na (0.04 wt.%) 1.12 wt.% Pt/HTO:Si powder tested in a ramp down mode at a space velocity of 20,000 h^{-1}.

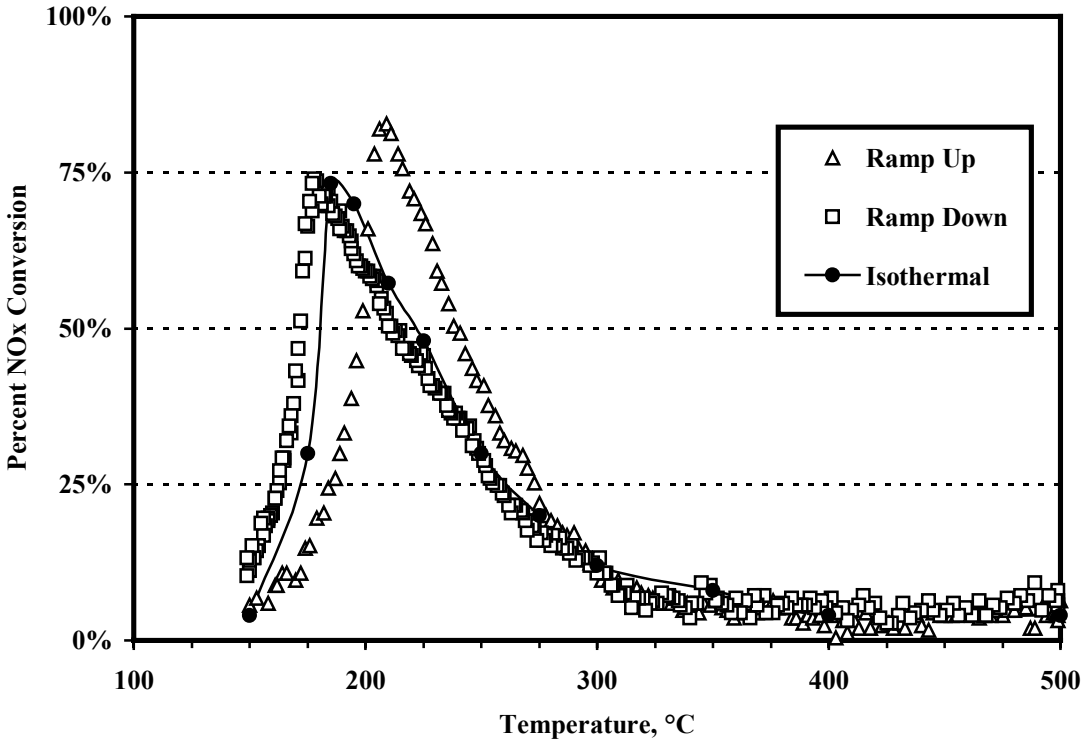

Figure 2. NOx conversion profiles for a low Na (0.04 wt.%) 1.12 wt.% Pt/HTO:Si powder tested in ramp up, ramp down, and isothermal steady state modes at a space velocity of 20,000 h^{-1}.

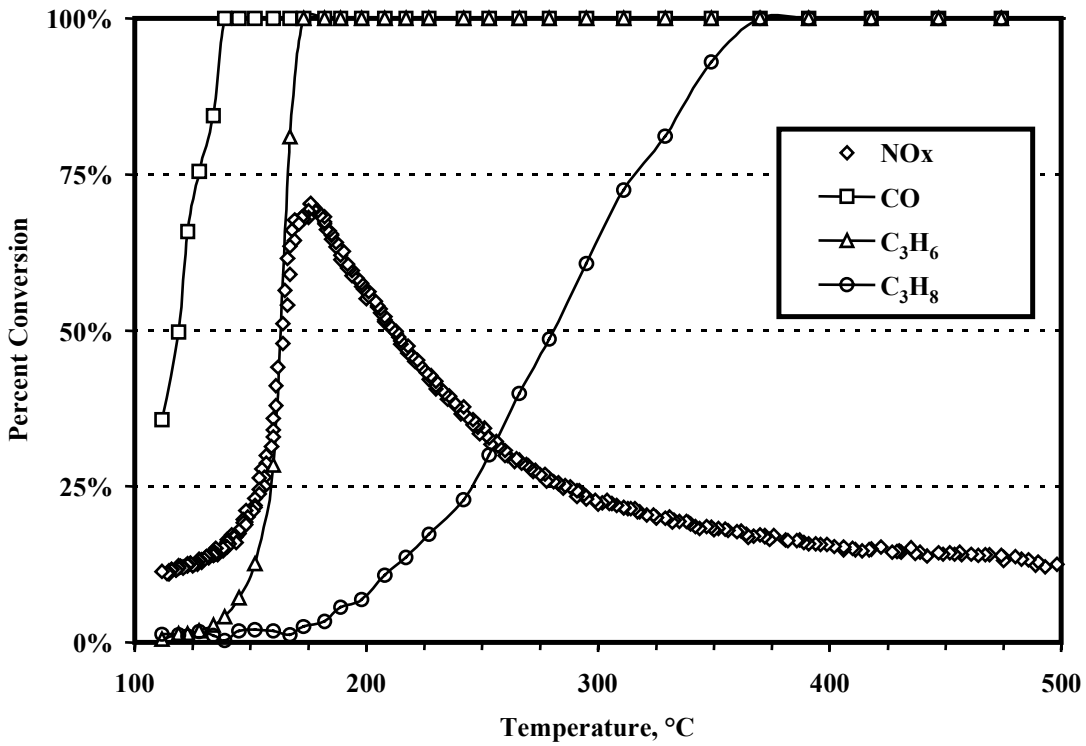

Figure 3. Conversion profiles for all species (CO, C_3H_6, C_3H_8, and NOx) for an anion exchanged low Na (0.01 wt.% Na) 0.95 wt.% Pt/HTO:Si powder tested in a ramp down mode at a space velocity of 20,000 h^{-1}.

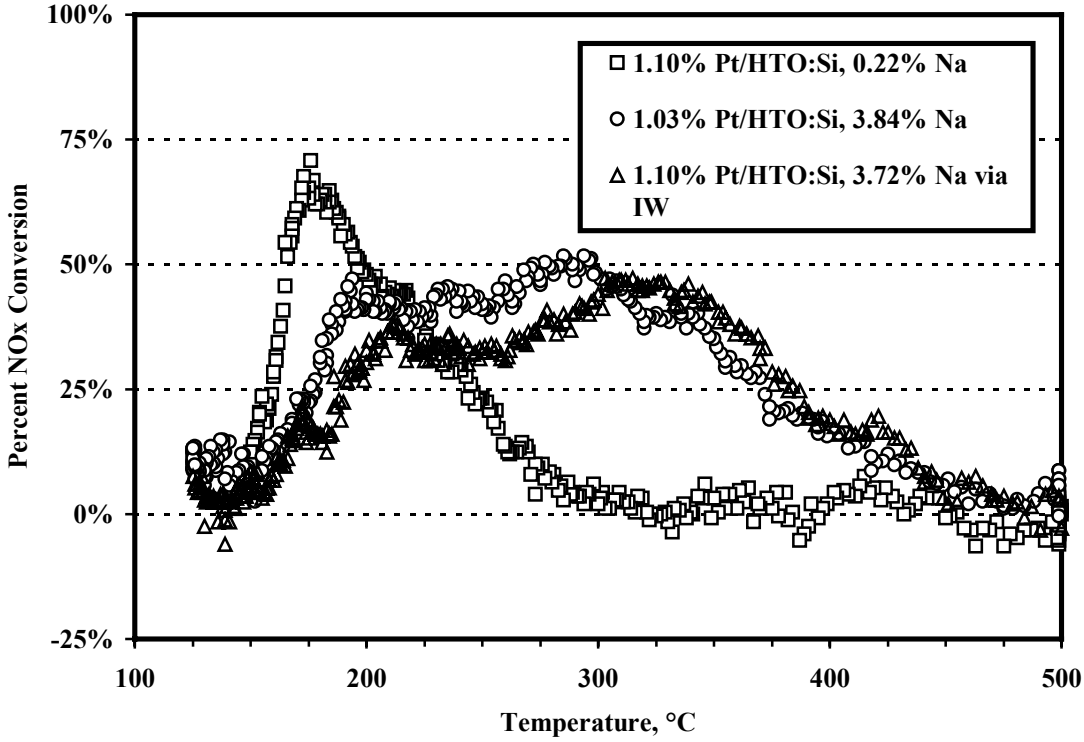

Figure 4. NOx conversion profiles comparing a low Na (0.22 wt.% Na) 1.10 wt.% Pt/HTO:Si powder with two high Na (nominal 3.8 wt.% Na) Pt/HTO:Si powders (nominal Pt loading of 1.0 wt.%) tested in ramp down modes at a space velocity of 20,000 h^{-1}.

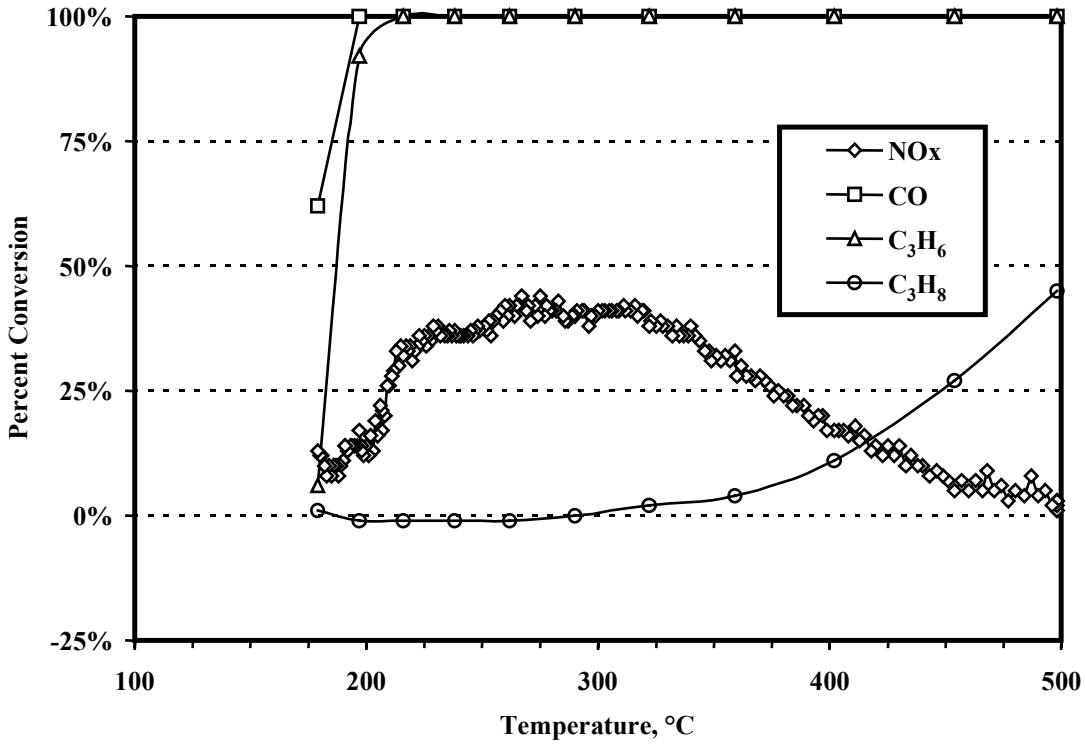

Figure 5. Conversion profiles for all species (CO, C_3H_6, C_3H_8, and NOx) for a high Na (3.89 wt.%) 0.90 wt.% Pt/HTO:Si powder tested in a ramp down mode at a space velocity of 20,000 h^{-1}.

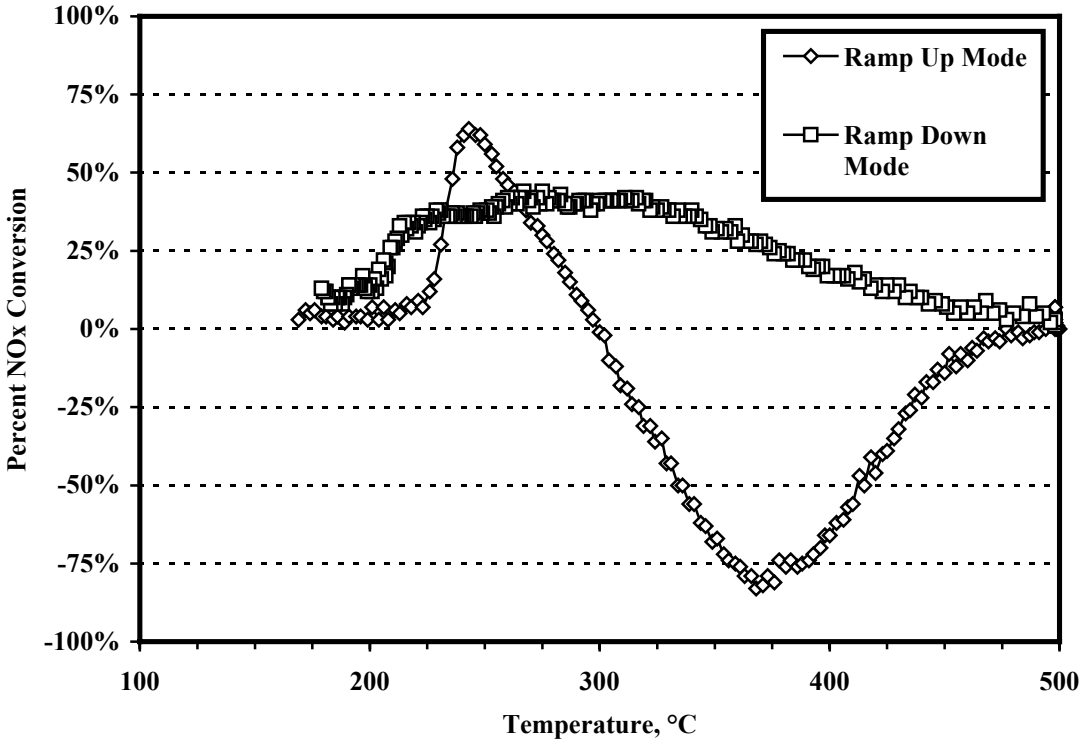

Figure 6. NOx conversion profiles for sequential ramp up and ramp down experiments using a high Na (3.89 wt.%) 0.90 wt.% Pt/HTO:Si catalyst and a space velocity of 20,000 h^{-1}. The large negative conversion observed during the ramp up mode experiment is clearly indicative of NOx desorbing from the catalyst.

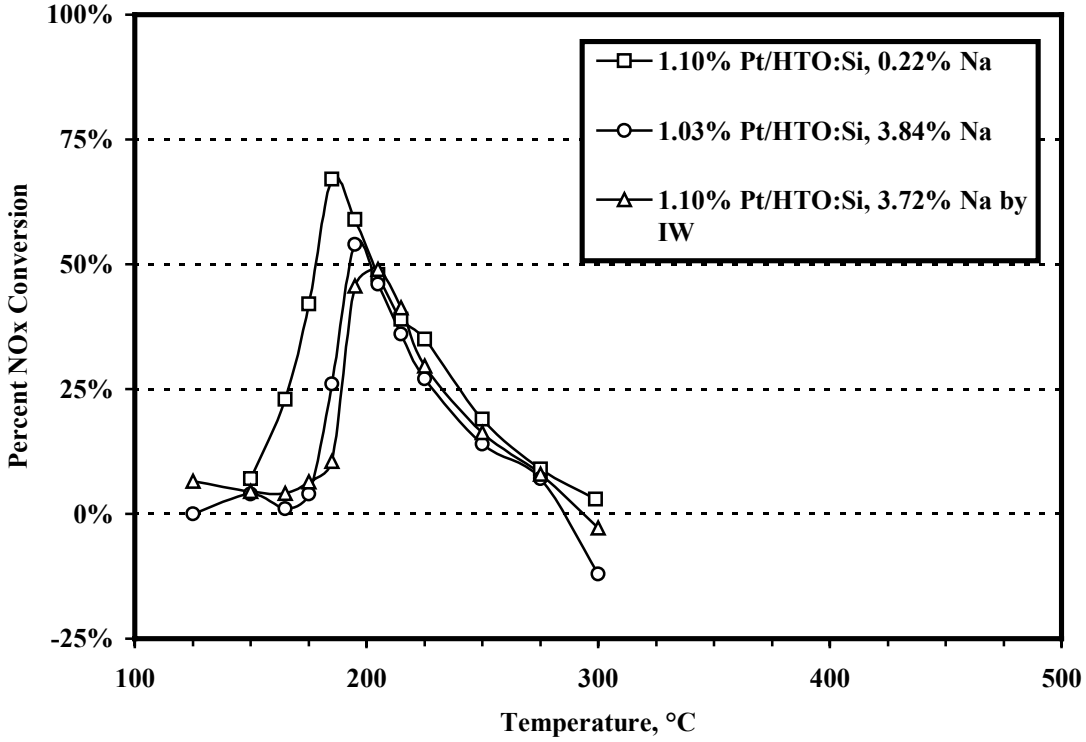

Figure 7. NOx conversion profiles for isothermal experiments using a space velocity of 20,000 h^{-1} and nominal 1 wt.% Pt/HTO:Si catalysts with various Na contents. High Na Pt/HTO:Si materials were prepared using both the standard technique and by the incipient wetness addition of Na to low Na Pt/HTO:Si catalysts.

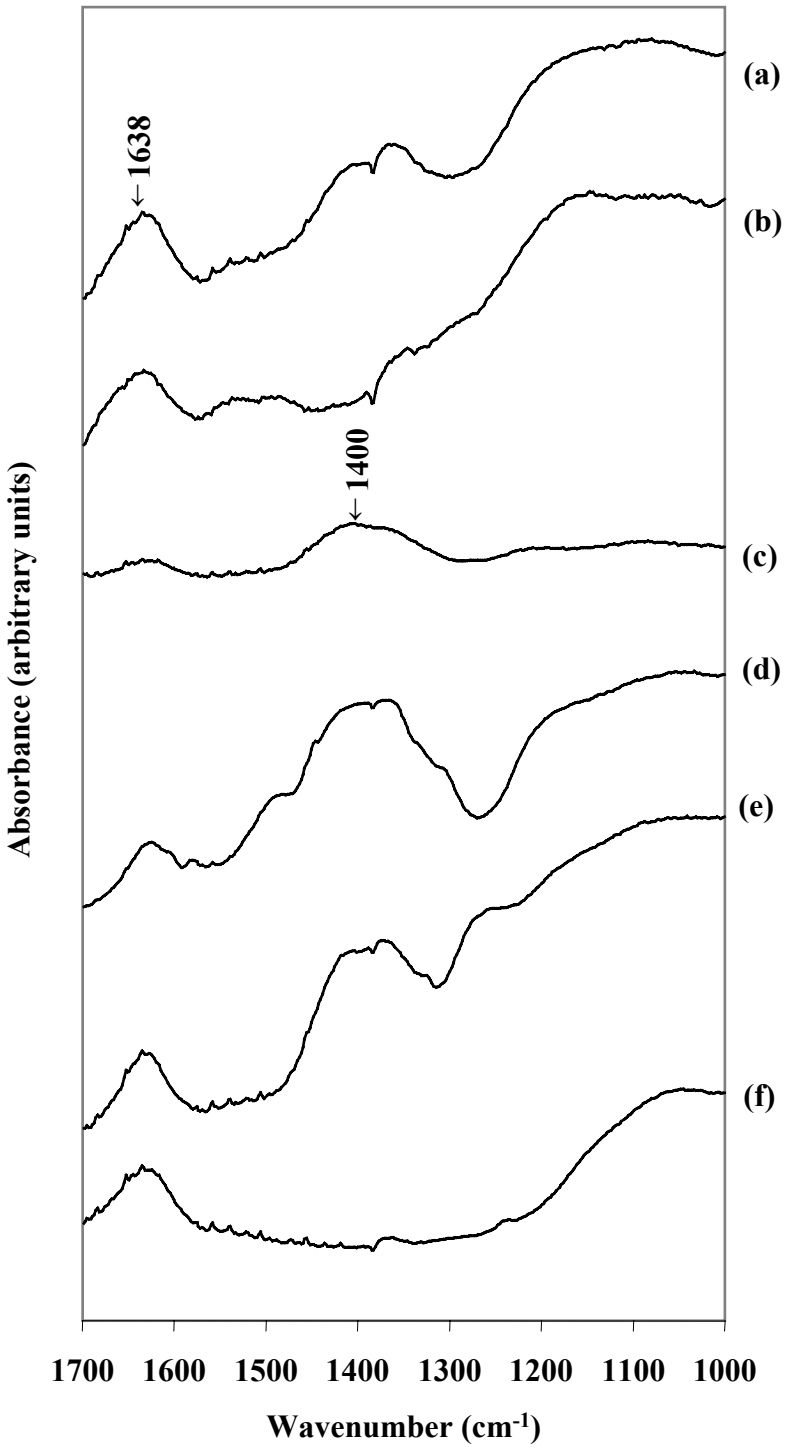

Figure 8. Diffuse reflectance FTIR spectra for high Na Pt/HTO:Si catalysts (as-calcined vs. after NOx uptake experiment) and various control samples: a) high Na (3.32 wt.%) 0.90 wt.% Pt/HTO:Si sample after NOx uptake experiment; b) high Na (3.32 wt.%) 0.90 wt.% Pt/HTO:Si sample in as-calcined form; c) difference spectra (a-b); d) 12.9 wt.% $NaNO_3$/HTO:Si control sample; e) 10.5 wt.% $NaNO_2$/HTO:Si control sample; and f) as-calcined HTO:Si support (0.31 wt.% Na).

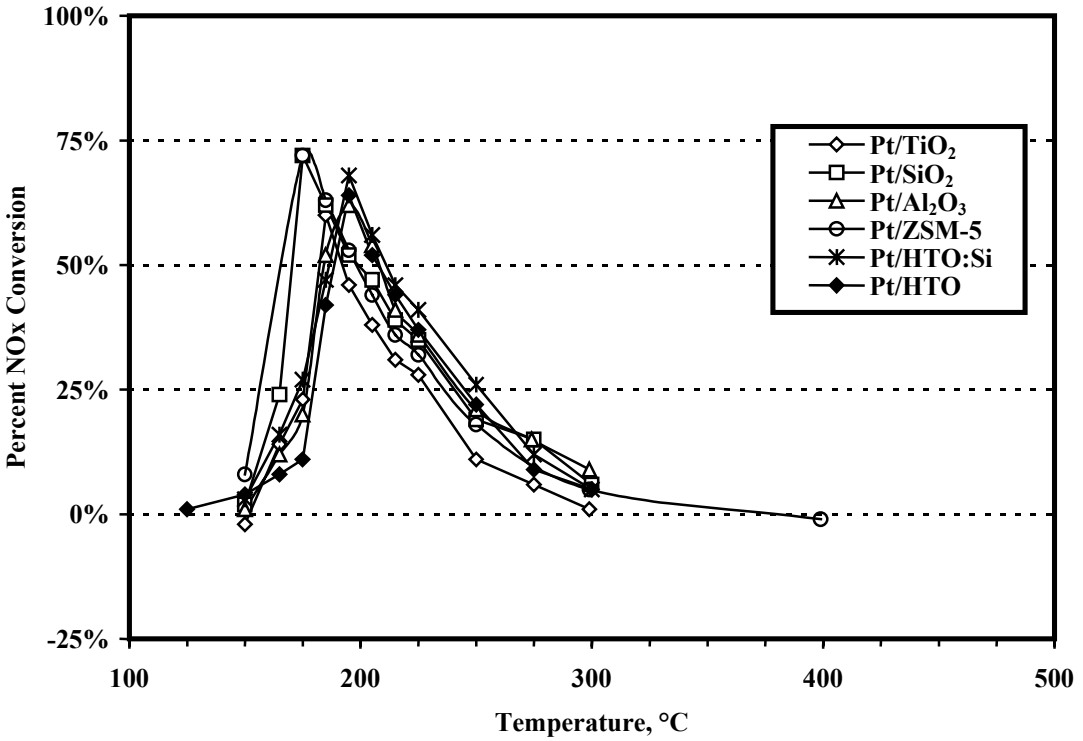

Figure 9. NOx conversion profiles for various supported Pt catalysts with a nominal Pt loading of 1.0 wt.%. All catalysts were tested using an isothermal test profile (ramp up mode) at a space velocity of 20,000 h^{-1}.

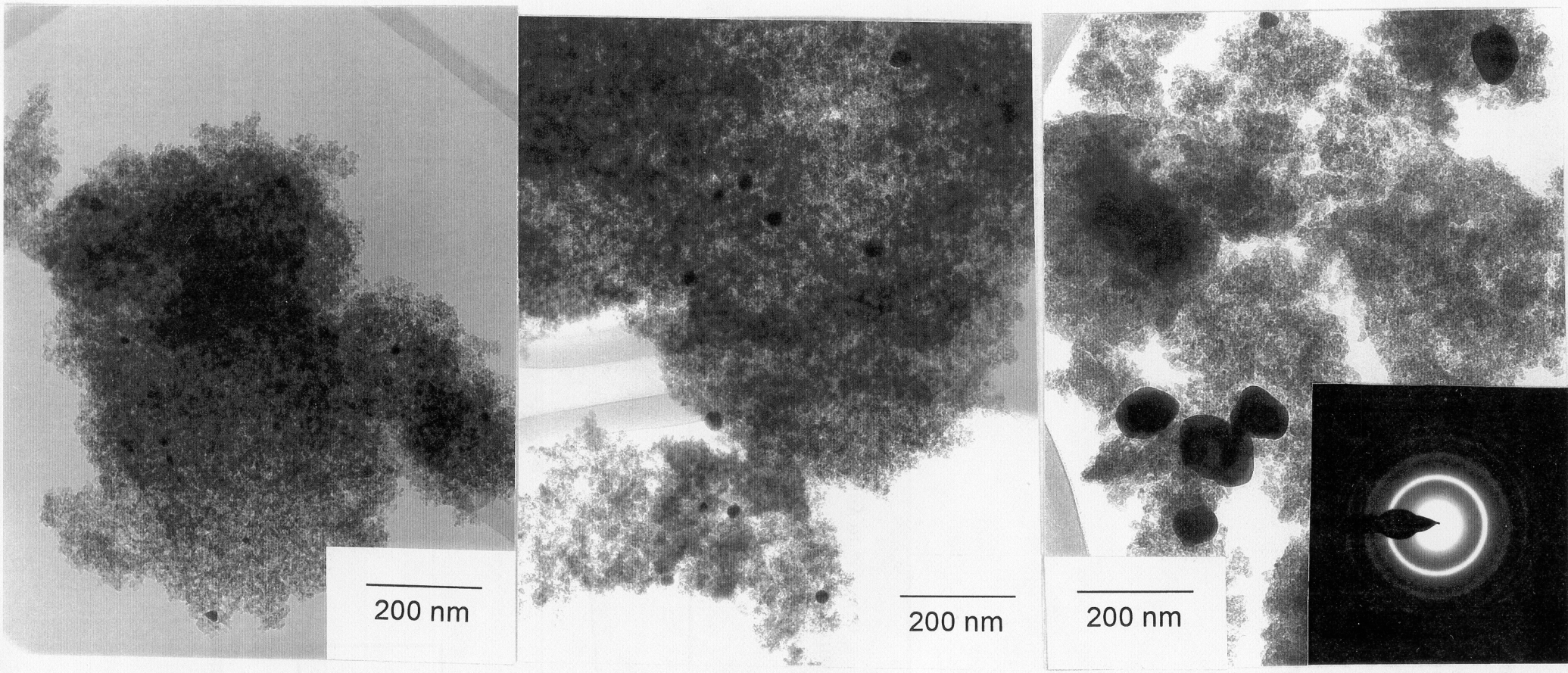

Figure 10. TEM photomicrographs of low Na (0.29 wt.%) 1.09 wt.% Pt/HTO:Si catalyst, including inset electron diffraction pattern representative of TiO_2 support phase.

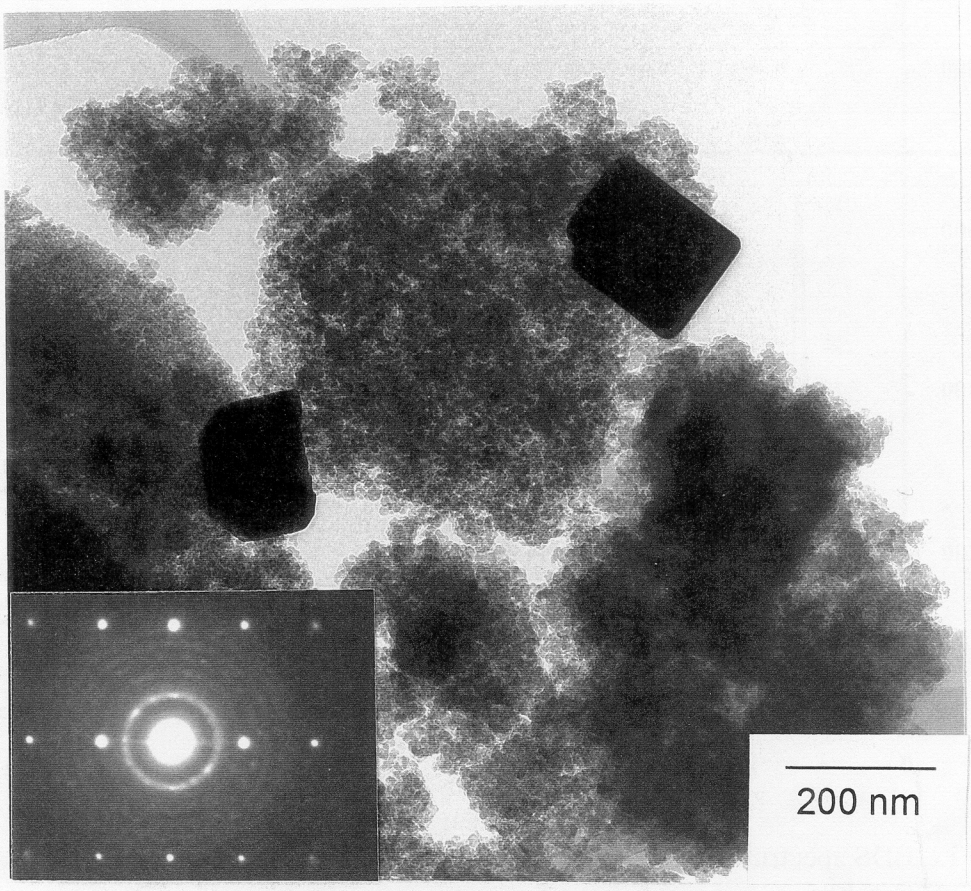

Figure 11. TEM photomicrograph of high Na (3.70 wt.%) 0.94 wt.% Pt/HTO:Si catalyst, including inset electron diffraction pattern representative of large single crystal ([112] orientation) Pt particles.

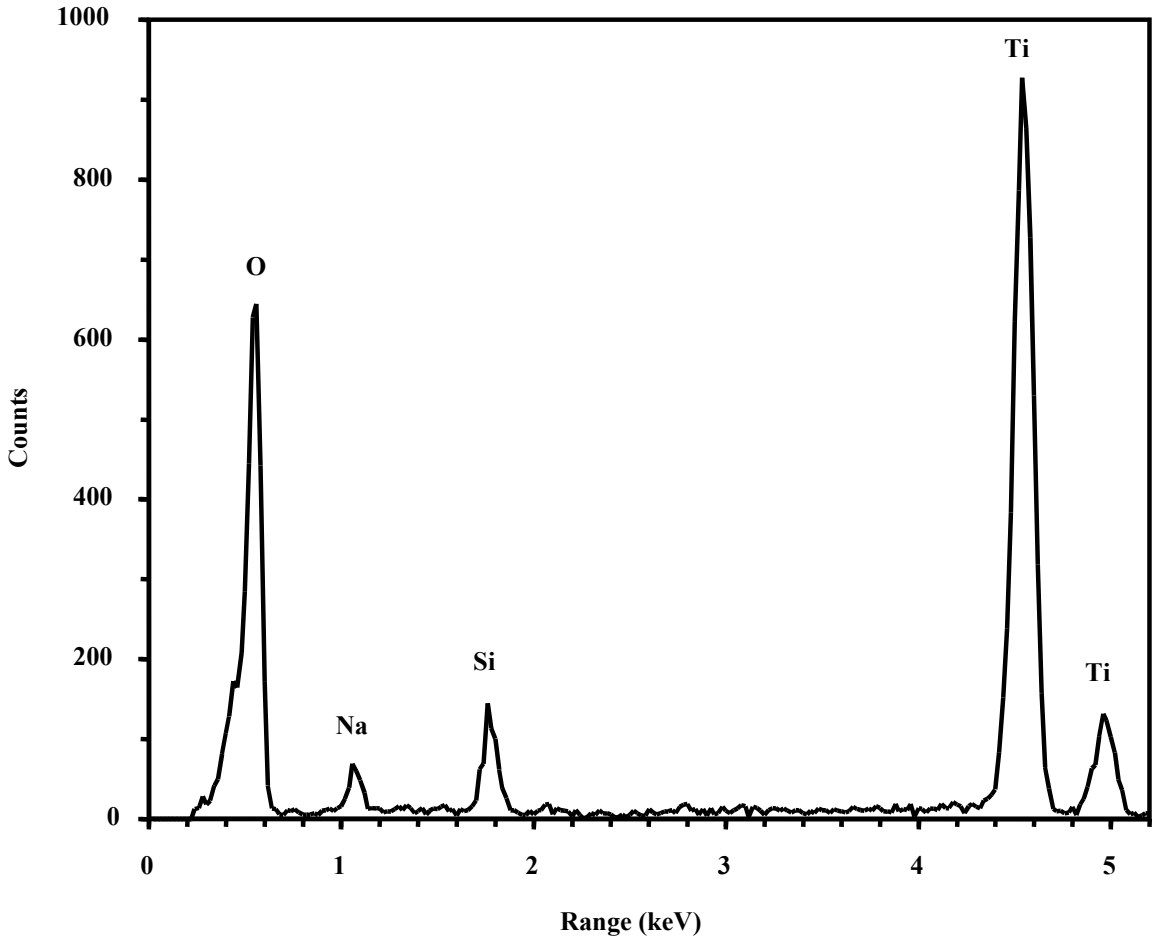

Figure 12. EDS spectrum of support phase composition for high Na (3.70 wt.%) 0.94 wt.% Pt/HTO:Si catalyst.

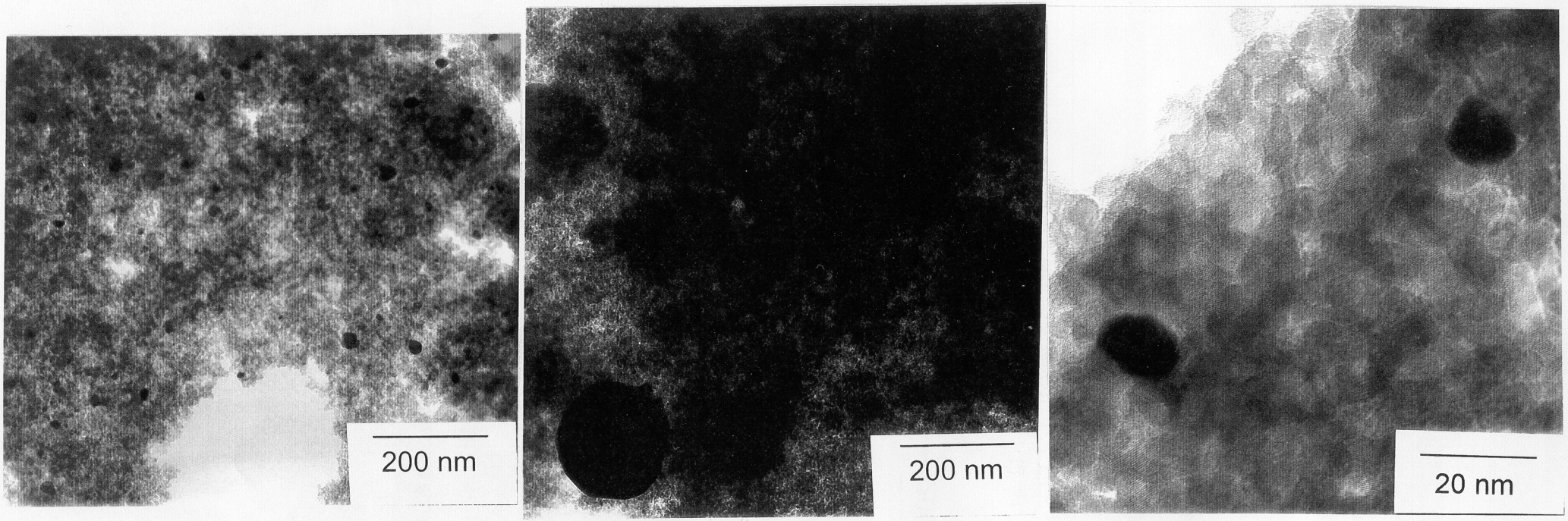

Figure 13. TEM photomicrographs of low Na (0.01 wt.%) 0.95 wt.% Pt/HTO:Si catalyst produced by anion exchange.

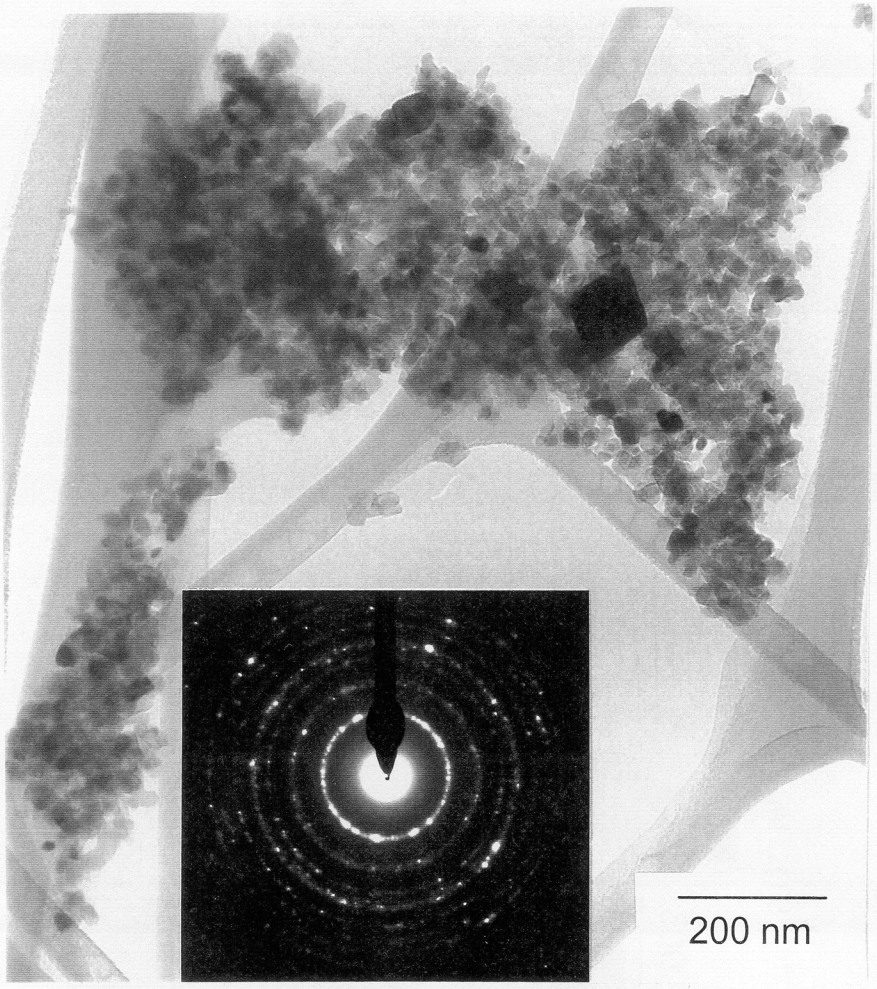

Figure 14. TEM photomicrograph of low Na (0.10 wt.%) 1.11 wt.% Pt/HTO catalyst, including inset electron diffraction pattern representative of TiO_2 support phase.

DISTRIBUTION:

Michael J. Royce
DaimlerChrysler Corporation, CIM 482-01-07
800 Chrysler Drive East
Auburn Hills, MI 48326-2757

Richard J. Blint
General Motors Corporation
Research and Development Center
MC 480-106-185
30500 Mound Road
Warren, MI 48090-9055

Byong K. Cho
General Motors Corporation
Research and Development Center
MC 480-106-185
30500 Mound Road
Warren, MI 48090-9055

John V. Cavataio
Ford Motor Company
Scientific Research Laboratories, MD-3179
2101 Village Road
P.O. Box 2053
Dearborn, MI 48121-2053

Robert H. Hammerle
Ford Motor Company
Scientific Research Laboratories, MD-3179
2101 Village Road
P.O. Box 2053
Dearborn, MI 48121-2053

Kathi Epping
U.S. Department of Energy
1000 Independence Ave. SW
EE-32
Washinton, DC 20585

Sandia Internal:

10	MS 1349	T.J. Gardner, 1846
1	MS 1349	D.L. Mowery, 1846
1	MS 1349	L.I. McLauglin, 1846
1	MS 1349	R.S. Sandoval, 1846
1	MS 1411	B.G. Potter, Jr., 1846
1	MS 9018	Central Technical Files, 8945-1
2	MS 0899	Technical Library, 9616
1	MS 0612	Review and Approval Desk, 9612 For DOE/OSTI